Effects of adverse sea conditions on propulsion and manoeuvring performance of low-powered ocean-going cargo ship

Sui, Congbiao; de Vos, Peter; Hopman, Hans; Visser, Klaas; Stapersma, Douwe; Ding, Yu

DOI
10.1016/j.oceaneng.2022.111348

Publication date
2022

Document Version
Final published version

Published in
Ocean Engineering

Citation (APA)
Sui, C., de Vos, P., Hopman, H., Visser, K., Stapersma, D., & Ding, Y. (2022). Effects of adverse sea conditions on propulsion and manoeuvring performance of low-powered ocean-going cargo ship. *Ocean Engineering*, *254*, Article 111348. https://doi.org/10.1016/j.oceaneng.2022.111348

Ocean Engineering 254 (2022) 111348

Contents lists available at ScienceDirect

Ocean Engineering

journal homepage: www.elsevier.com/locate/oceaneng

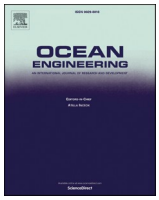

Effects of adverse sea conditions on propulsion and manoeuvring performance of low-powered ocean-going cargo ship

Congbiao Sui [a,b], Peter de Vos [b], Hans Hopman [b], Klaas Visser [b], Douwe Stapersma [b], Yu Ding [a,*]

[a] College of Power and Energy Engineering, Harbin Engineering University, Harbin, 150001, China
[b] Faculty of Mechanical, Maritime and Materials Engineering, Delft University of Technology, 2628, CD Delft, the Netherlands

ARTICLE INFO

Keywords:
Adverse sea
Low-powered ship
Minimum propulsion power
Engine dynamic performance
Ship operational safety

ABSTRACT

Current EEDI (Energy Efficiency Design Index) regulations striving to reduce the installed engine power on new ships for a low EEDI may lead to underpowered ships having insufficient power when operating in adverse sea conditions. In this paper, the operational safety of a low-powered ocean-going cargo ship operating in adverse sea conditions has been investigated using an integrated ship propulsion, manoeuvring and sea state model. The ship propulsion and manoeuvring performance, especially the dynamic engine behaviour, when the ship is sailing in heavy weather and turning into head sea, have been studied. According to the results, the dynamic engine behaviour should be considered when assessing the ship operational safety, as the static engine operating envelope is inadequate for the safety assessment. The impact of PTO/PTI (power-take-off/in) operation and changing propeller pitch on the ship thrust availability in adverse sea conditions have also been investigated. To protect the engine from mechanical and thermal overloading, compressor surge and over-speeding during dynamic ship operations and/or in high sea states, the engine and propeller should be carefully controlled. The paper shows that if in (heavy) adverse weather the propeller pitch can be reduced or if the shaft generator can work as a motor (PTI), more thrust can be developed which can significantly improve the operational safety of the ship.

1. Introduction

1.1. Problem definition

Ocean shipping, which carries more than 80% of world trade by volume, remains the backbone of international merchandise trade (UNCTAD, 2019). According to the Third IMO Greenhouse Gas Study, around 3% of annual greenhouse gas emissions come from shipping on average from 2007 to 2012, and it is projected that CO_2 emissions from maritime transport could increase by 50%–250% by 2050 (Smith et al., 2015). Aiming at promoting the application of more energy efficient equipment and engines on ships to reduce the environmental impact from shipping industry, the Energy Efficiency Design Index (EEDI) as an important technical measure has been made mandatory for new ships by the International Maritime Organization (IMO) (MEPC, 2011). New ship designs need to meet the EEDI requirements, i.e., the attained EEDI of the ship should be no more than the required EEDI for their ship types. Compared to adopting innovative ship design concepts and energy efficient technologies, a technically easy and effective solution to meet the EEDI requirement is to lower the installed engine power (Mundt et al., 2019). However, if reducing the installed engine power has been chosen to achieve a small EEDI, it could lead to an underpowered ship, which is believed to be vulnerable and unsafe as the engine may not be capable of providing sufficient power for ship propulsion and steering under adverse weather conditions (Papanikolaou et al., 2016).

According to a statistical analysis of marine accidents (Shigunov et al., 2019; Ventikos et al., 2018), it is believed that quite a number of underpowered ships are currently sailing at sea worldwide, especially ships with small EEDI that is achieved by simply reducing the installed engine power. To prevent an irrational reduction of the installed engine power, the 2013 interim guidelines for the minimum installed propulsion power to maintain the manoeuvrability of ship in adverse sea conditions have been adopted by IMO in 2013 (MEPC, 2013) and further updated (strengthened) in 2015 (MEPC, 2015). The consolidated version of the 2013 interim guidelines (MEPC, 2017) is the only regulatory requirement that addresses the ships minimum propulsion power issues in adverse sea conditions. Tankers, bulk carriers and combination carriers, which are considered the most critical ship types concerning the power sufficiency for steering in adverse weather conditions

* Corresponding author.
E-mail address: dingyu@hrbeu.edu.cn (Y. Ding).

https://doi.org/10.1016/j.oceaneng.2022.111348
Received 21 September 2021; Received in revised form 9 February 2022; Accepted 15 April 2022
Available online 28 April 2022

Nomenclature

Abbreviations

AC	alternating current; air cover
AG	auxiliary generator
Aux. Eng	auxiliary engine
Aux. Gen	auxiliary generator
EEDI	energy efficiency design index
GB	gearbox
Gen	generator
IMO	International Maritime Organization
MCR	maximum continuous rating
PTO	power take off
PTI	power take in

Roman Symbols

C_{XA}, C_{YA}, C_{NA}	wind forces and moment coefficients (−)
C_{XW}, C_{YW}, C_{NW}	waves forces and moment coefficients (−)
C_T^*	propeller thrust coefficient (−)
H_S, $H_{1/3}$	Significant wave height (m)
h_a	wave amplitude (m)
I_z	moment of inertia of the ship (kg·m2)
J	propeller advance coefficient (−)
J_z	added moment of inertia of the entrained water (kg·m^2)
m_x, m_y	added mass of the entrained water in x-direction and y-direction (kg)
M_{del}	delivered torque to propeller (Nm)
M_{eng}	engine torque (Nm)
M_{prop}	propeller torque (Nm)
M_{shaft}	shaft torque (Nm)
N	yaw moment around z-axis (Nm)
p	pressure (Pa)
p_{max}	maximum in-cylinder pressure (Pa)
r	ship yaw rate around the z-axis (rad/s)
t	propeller thrust deduction fraction (−); time (s)
tP	propeller thrust deduction fraction (−)
tR	steering resistance deduction factor of rudder (−)
T	temperature (K)
Tp	peak wave period (s)
Tv	average wave period (s)
$Tprop$	propeller thrust (N)
U	velocity (m/s)
u	velocity in x-axis direction (m/s)
uA	propeller advance speed (m/s)
v	velocity in y-axis direction (m/s)
w	propeller wake fraction (−)
xG	longitudinal distance between the centre of buoyancy and mid ship (m)
X	force in x-axis direction (N); fuel rack position (−)
Y	force in Y-axis direction (N)

Greek symbols

α_R	effective rudder inflow angle (deg)
β	drift angle of the ship (deg)
β^*P	hydrodynamic pitch angle of propeller (deg)
δ	rudder angle (deg)
∇	ship displacement volume (m^3)
χ	encounter angle (deg)
λ	air excess ratio (−); wave length (m)
A_R	aspect ratio of rudder (−)
ψ	ship heading angle (deg)

Subscripts

A, a	air
COM	compressor
EO	exhaust valve open
EV	exhaust valve
H	ship hull
IR	inlet receiver
OR	outlet receiver
P	propeller
R	rudder
S	ship
SI	surge index
TC	turbocharger
TUR	turbine
W	waves
x	in x-axis direction
y	in y-axis direction
z	around z-axis

(Psaraftis, 2019), have been addressed in the 2013 interim minimum power guidelines. The current guidelines apply to the above-mentioned ships with a capacity of equal or above 20,000 DWT. Due to the disputed sufficiency of the 2013 interim guidelines, two large research projects, i.e., SHOPERA and JASNAOE (among several others), have been conducted trying to revise and improve the minimum power guidelines (IMO, 2016a, 2016b; Shigunov, 2018). However, the research project conclusions are considered not mature enough to revise the guidelines, and these have not been finalized to date (IMO, 2019; Psaraftis, 2019). Moreover, currently there is no minimum power guideline applicable for ships with a capacity less than 20,000 DWT and studies for these ships are still ongoing.

As these developments have raised serious safety concerns for underpowered ships, many researches have been conducted to assess ship safety in adverse sea conditions. In (Shigunov, 2018), the required criteria, measures and standards of manoeuvrability of ships in adverse weather conditions have been addressed and a practical assessment procedure has been proposed. In (Shigunov, 2020), the practical assessment of ship manoeuvrability in adverse conditions and the availability of experimental, numerical and empirical methods for evaluating the time-average wind and waves induced forces and moments, etc., have been discussed. Shigunov's work is part of the previously mentioned project SHOPERA, of which the goal was trying to revise the current minimum propulsion power guideline and the assessment procedure of ship manoeuvrability in adverse weather conditions. Nevertheless, they mainly consider what is happening outside of the ship hull in adverse sea conditions, while this research mainly focuses on what is happening inside the ship, especially the dynamic behaviour of the engine. When sailing in adverse weather conditions, the ship propulsion and manoeuvring behaviour will be influenced by not only the wind and waves induced steady forces but also the propeller wake variation and even propeller ventilation and emergence in harsher weather. Consequently, the interactions between the ship propulsion system, the ship, the waves and winds, etc., in high sea states are very complex and highly dynamic. Having a detailed insight of these complex and highly dynamic interactions between the inside and outside of the ship is the crux of the evaluation of ship operational safety in adverse sea conditions. In (Taskar et al., 2016), the effects of propeller wake variation and emergence on the engine-propeller dynamics and ship propulsion performance when sailing in waves have been investigated. In (Yum et al., 2017), the simulation of a two-stroke marine diesel engine for ship propulsion in waves has been conducted based on a propulsion system model in waves; and the effects of propeller inflow velocity variations and propeller emergence on the transient performance of the

engine have been investigated. A detailed crank-angle engine model has been used in (Taskar et al., 2016) and (Yum et al., 2017) to investigate the wave effects on the engine dynamics, however, only ship propulsion in waves has been considered, while ship manoeuvring in wind and waves when sailing in adverse sea has not been taken into account. In (Aung and Umeda, 2020), based on the simulation model for ship manoeuvring in adverse weather conditions, the effects of different sea states (indicated by Beaufort No.), ship initial forward speed and engine SMCR power on ship manoeuvring behaviour in adverse weather conditions have been investigated; the influence of the emergence of propeller and rudder has been considered. However, in (Aung and Umeda, 2020), a simplified engine model neglecting the engine thermodynamics process has been used, and only engine torque has been modelled and it is assumed to be linearly proportional to the amount of the injected fuel into the engine, with the consideration of the static engine load limits. So, the work in (Aung and Umeda, 2020) mainly focuses on the ship manoeuvrability and seakeeping in wind and waves; while it does not provide a detailed insight of the engine behaviour when ships are manoeuvring in adverse sea conditions. Since the ship safety in adverse weather conditions is highly related to the engine operational safety, a detailed and systematic investigation on the engine behaviour (including both static and dynamic behaviour) under various operating conditions is important and necessary (Holt and Nielsen, 2021; Sui et al., 2021), however, the research in this respect is still limited.

1.2. Approach

There are many challenges in the study of ship operational safety in adverse sea conditions, especially when taking the engine behaviour, ship manoeuvrability and seakeeping into account as a whole system. Normally, a collaboration of experimental and simulation methods is needed, especially when investigating the ship manoeuvring and seakeeping in waves, which is a difficult hydrodynamic problem (Shigunov, 2019). In this research, the needed experimental data are obtained from our cooperation partners, including the engine manufacturer and the shipyard; while the numerical calculation data of waves induced steady forces in different sea states are obtained from the published literatures. This research aims to develop an integrated first principle and modular simulation model that is capable of providing detailed insight in the complicated and dynamic interactions between engine, propeller, ship and wind and waves, etc., when the ship is sailing and manoeuvring in adverse sea conditions. The integrated system model is developed from first principles at different levels as much as possible, so, it is able to predict the right trends of both static and dynamic ship behaviour under various operating conditions. With the model calibration using ample real ship data, adequate and reasonable model verification, and model validation using experimental and sea trial test data, the model is assumed to be sufficiently accurate. Moreover, the model is easy to use and is able to run on a normal personal computer with an acceptable calculation speed (calculation time being a few percent of real time), without the need of a high-performance computer.

To provide a detailed insight in the engine dynamic behaviour in various operating conditions, a Mean Value First Principle Parametric (MVFPP) engine model was developed and introduced in (Sui et al., 2021) and has been applied in this research. To investigate ship manoeuvrability in adverse sea, an empirical 3DOF ship manoeuvring model and a wind and waves model have been applied. In this research, when investigating the ship propulsion and manoeuvring performance, especially the engine dynamic performance, in adverse sea conditions, it is assumed that the ship sails at the design loading condition in open sea, and the ship heaving and pitching motions are left out of consideration. The rolling motion caused by ship turning in normal sea condition is considered negligible for the ocean-going cargo ship. Also, ship rolling caused by wind and waves in adverse sea conditions will be left out of consideration, as the impact of rolling motion on the hydrodynamic manoeuvring forces and moments by the propeller, rudder and hull is assumed negligible for the ocean-going cargo ship, which generally has single propeller and single rudder at the centreline of the ship. So, the 3DOF ship manoeuvring model (surge, sway and yaw) is considered sufficient for investigating the engine behaviour during ship propulsion and manoeuvring in adverse sea conditions. Depending on different ways that the components of external forces and moments acting on the ship are expressed and parametrised, the ship manoeuvring models can be divided as: the whole ship models and the modular models (Liu, 2017). The whole ship models, such as the Abkowitz model (Abkowitz, 1964), address the hull, propeller and the rudder together as a black box without considering the interactions between them; and the hydrodynamic forces and moments are expressed in Taylor series as functions of kinematic parameters and rudder angles without clear physical meanings. The modular models, such as the MMG model proposed and developed by the Mathematical Modeling Group of the Society of Naval Architects of Japan (Inoue et al., 1981; Kijima et al., 1990; Ogawa et al., 1977; Yasukawa and Yoshimura, 2015), consider the component hydrodynamic forces and moments caused by the hull, propeller, rudder and also the hull-propeller-rudder interactions. So, the modular manoeuvring models are first principle and have explicit physical meanings. Using the modular models, the effects of the physical components including the hull, propeller, rudder, the interactions between them and even the external disturbances (such as wind and waves) on the ship manoeuvring performance can be analysed separately and/or in combination, with the possibility of using different methods (experimental, numerical or empirical) (Aung and Umeda, 2020; Yasukawa and Sakuno, 2020; Zhang et al., 2019).

In this paper, the modular and first principle MMG ship manoeuvring model, which is able to provide a satisfactory insight of the physical phenomena of ship manoeuvring, has been used for the research. To determine the hydrodynamic coefficients in the ship manoeuvring model, empirical methods based on a limited number of main particulars of the ship have been applied. When taking the influences of wind and waves in adverse sea conditions into account, only wind- and waves-induced steady forces, including ship resistance increase, wind- and waves-induced steady lateral forces and yaw moments, and waves-induced propeller wake fluctuations will be considered, while the influences of possible propeller ventilation and propeller emergence will be left out of scope. Currently there are no well-established empirical formulae for estimating the wave-induced steady forces, especially the waves-induced lateral force and yaw moment, so, the experimental and numerical results from literature in this regard will be used in this paper.

1.3. Objective

The objective of this paper is to provide a detailed insight of ship propulsion and manoeuvring performance, especially engine dynamic behaviour, of the low-powered ocean-going cargo ship when operating in adverse sea conditions; however, the research in this regard is limited in published literature. The main goals and outline of this paper are:

1) It will be explained why the benchmark chemical tanker could well be a low-powered or even underpowered ship under present rules. The definition of adverse sea conditions and the safety criteria of ship propulsion and manoeuvring in adverse sea for the benchmark chemical tanker according to the current 2013 interim minimum power guidelines will be introduced (Section 2);
2) The integrated ship propulsion, manoeuvring and sea state model, including the 3DOF ship manoeuvring model, the model of wind- and waves-induced steady forces and moments, and the model of propeller wake fluctuation in waves, will be presented (Section 3);
3) The 3DOF ship manoeuvring model of the benchmark chemical tanker will be validated using the sea trial test data of the ship. The model of wind and waves will be verified by simulating ship turning in different sea state with different initial velocities (Section 4);

4) Based on the integrated ship propulsion, manoeuvring and sea state model, the ship propulsion and manoeuvring performance when sailing in heavy weather and turning to head sea will be investigated in detail. The influence of some operational measures, such as changing propeller pitch and using PTO/PTI, on the ship thrust envelope will also be investigated (Section 5);
5) Conclusions of the research in this paper and recommendations for future research will be provided (Section 6).

2. Low-powered benchmark ship and adverse sea conditions

2.1. Low-powered ocean-going chemical tanker

The benchmark 13,000 DWT Chemical Tanker 'Castillo de Tebra' (Fig. 1) investigated in (Sui et al., 2019, 2020, 2021) will be chosen and applied again in this paper to investigate the propulsion and manoeuvring performance of low-powered ocean-going cargo ship in adverse sea conditions. The main engine of the benchmark chemical tanker is a low speed two-stroke marine diesel engine, and the three auxiliary engines generating electric power are four-stroke medium speed diesel engines. The ship has a controllable pitch propeller (CPP) and a shaft generator (power take off, PTO), which are driven by the main engine; and three auxiliary generators driven by the auxiliary engines. In (Sui et al., 2020), it has been conceptually updated such that the shaft generator can also work as a shaft motor (power take in, PTI). The layout of the benchmark chemical tanker propulsion system and electric generating system is shown in Fig. 2. The information of the ship and its engines are presented in Table 1 and Table 2.

The 13,000 DWT benchmark chemical tanker, which has a low EEDI of 9.92 gCO_2/ton•mile, meets the EEDI requirement (10.59 gCO_2/ton•mile) of phase 2 (1 Jan 2020–31 Dec 2024) and is very close to the EEDI requirement (9.91 gCO_2/ton•mile) of phase 3 (1 Jan 2025 and onwards). According to the EEDI technical file of the benchmark chemical tanker, which is submitted to class for final verification for the attained EEDI at the delivery stage, the 2013 interim minimum power guidelines (RESOLUTION MEPC.232(65)) (MEPC, 2013) has been applied for assessing whether the ship has sufficient power to maintain the manoeuvrability in adverse conditions. However, currently there are no minimum power guidelines applicable for ships with capacity less than 20,000 DWT including the benchmark chemical tanker. If applicable, according to the level 1 assessment of the 2013 interim guidelines, i.e., the minimum power lines assessment, the installed MCR of the main engine of the benchmark chemical tanker should not be less than 4148.7 kW, so, the installed engine power (4170 kW) on the ship meets this minimum power requirement.

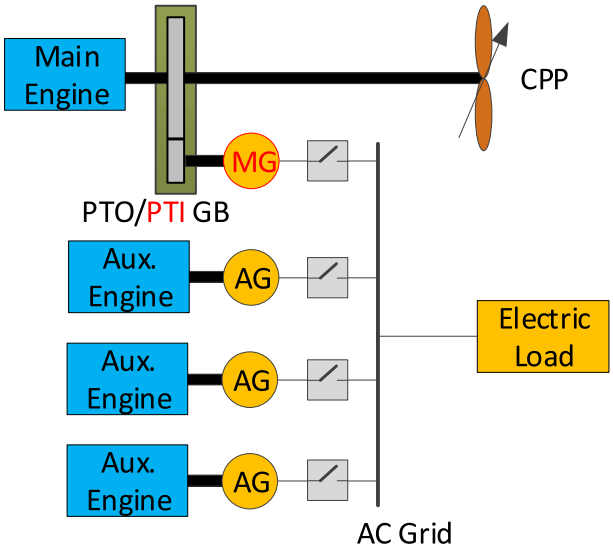

Fig. 2. Layout of the updated chemical tanker propulsion system and electric generating system (Sui et al., 2020).

Table 1
Ship particulars of the benchmark chemical tanker (Sui et al., 2020).

Length Between Perpendiculars (m)	113.80
Breadth Molded (m)	22.00
Depth Molded (m)	11.40
Design Draught (m)	8.50
Design Displacement (m^3)	16,988
Dead Weight Tonnage (ton)	13,000
Design Ship Speed (kn)	13.30

However, according to the latest amended guidelines (MEPC.1/Circ.850/Rev.2) (MEPC, 2017), the minimum installed engine power of the chemical tanker is 6807.8 kW, which is much higher than the MCR power (4170 kW) of the main engine installed on the ship. So, if applicable, according to the amended 2013 guidelines, the benchmark

Fig. 1. 13,000 DWT Chemical Tanker 'Castillo de Tebra' (Sui et al., 2019).

Table 2
Particulars of the main engine and auxiliary engines (Sui et al., 2020).

Parameters	Main Engine	Auxiliary Engine
Engine Type	MAN 6S35ME-B9.3-TII (2-stroke)	DAIHATSU 6DE-18 (4-stroke)
Number of engines (−)	1	3
Rated Power (kW)	4170	750
Rated Speed (rpm)	167	900
Stroke (m)	1.55	0.28
Bore (m)	0.35	0.185
Mean Effective Pressure (MPa)	1.67	2.21

chemical tanker would be a low-powered or even underpowered ship as it cannot meet the latest minimum power requirement. On the other hand, if the installed engine on the same ship is replaced by a larger engine with power of 6810 kW, the ship design speed will then increase from 13.30 knots to 15.80 knots, and as a result the EEDI of the ship will increase from 9.92 to as high as 14.00, which cannot meet the EEDI requirement even for phase 0 (11.97 gCO_2/ton•mile) anymore.

2.2. Adverse sea conditions and safety criteria

According to the current 2013 interim minimum power guidelines (MEPC, 2017), the adverse sea conditions for different ship sizes are defined by the corresponding wind speed and the significant wave height as shown in Table 3. For ships having length shorter than 200 m, the adverse sea condition is defined with the wind speed of 15.7 m/s and significant wave height of 4.0 m, and the corresponding Beaufort number (BF) is 7 according to the World Meteorological Organization (WMO, 2019). For ships having length longer than 250 m, the adverse sea condition is defined with the wind speed of 19.0 m/s and significant wave height of 5.5 m, and the corresponding Beaufort number (BF) is 8. For ships having length between 200 and 250 m, the corresponding wind speed and significant wave height are linearly interpolated according to the ship's length.

According to level 2 assessment of the current guidelines for minimum propulsion power, i.e., the simplified assessment, the safety assessment criteria is based on the principle that, '*if the ship has sufficient installed power to move with a certain advance speed in head waves and wind, the ship will also be able to keep course in waves and wind from any other direction*' (MEPC, 2017). The required ship advance speed sailing in head wind and waves should be the larger of: minimum navigational speed or the minimum course-keeping speed. In the current guidelines, the minimum navigational speed is set to 4.0 knots, with which the ship is considered to be able to leave coastal area within sufficient time before the storm escalates. The minimum course-keeping speed is selected based on ship design parameters, such as the rudder area and lateral windage area, etc., which have significant impact on the course-keeping performance of the ship in adverse see conditions. For details of the estimation procedure of the minimum course-keeping speed, refer to (MEPC, 2017).

Note that, the above definition of adverse conditions in the current guidelines are applicable to ships (bulk carriers, tankers and combination carriers) with a size equal to or more than 20,000 DWT. However, in this paper, for the moment it is assumed that the guidelines are also applicable to the benchmark chemical tanker, which has a capacity of 13,000 DWT. The specified adverse condition for the benchmark chemical tanker is the sea condition with Beaufort number of 7. The required advance speed of the benchmark chemical tanker in head wind and waves according to the current guidelines is 6.4 knots.

Table 3
Adverse sea conditions defined for different ship sizes by existing guidelines (MEPC, 2017).

Ship's length L_{PP} (m)	Wind speed (m/s)	Peak wave period T_P (s)	Significant wave height H_S (m)	Beaufort number (BF)
$L_{PP} < 200$	15.7	7.0 to 15.0	4.0	7
$200 \leq L_{PP} \leq 250$	Parameters linearly interpolated according to ship's length L_{PP}			
$L_{PP} > 250$	19.0	7.0 to 15.0	5.5	8

3. Integrated ship propulsion, manoeuvring and sea state model

The MVFPP (Mean Value First Principle Parametric) two-stroke marine diesel engine model and ship propulsion model of the benchmark chemical tanker introduced in (Sui et al., 2021) has been integrated with the ship manoeuvring model and sea state model. The layout of the integrated ship propulsion, manoeuvring and sea state model is shown in Fig. 3.

3.1. 3DOF ship manoeuvring model

To express and analyse ship's motions and the hydrodynamic forces, a convenient coordinate system, including the earth-fixed and body-fixed coordinate systems, needs to be established first. The North-East-Down (NED) coordinate system (O_0, x_0, y_0, z_0) has been used as the earth-fixed reference system, in which the x axis points towards the north, the y axis towards the east and the z axis downwards normal to the Earth's surface (Fossen and Wiley, 2011). The origin of the earth-fixed coordinate system (O_0) could be located at the start point of the ship's operation. The Bow-Starboard-Down coordinate system (O, x, y, z) with origin O fixed on the centre of gravity of the ship G is selected as the body-fixed reference system of the ship. The earth-fixed and body-fixed coordinate systems of MMG manoeuvring model and the coordinate system of the wind and waves are illustrated in Fig. 4. It is assumed that the wind and waves come from the same direction.

According to (Kijima et al., 1990), the equations of the ship's 3DOF dynamic motions are expressed by equation (1).

$$\left.\begin{array}{l}(m+m_x)\cdot\dot{u}-(m+m_y)\cdot v\cdot r=X\\(m+m_y)\cdot\dot{v}+(m+m_x)\cdot u\cdot r=Y\\(I_z+J_z)\cdot\dot{r}=N\end{array}\right\} \quad (1)$$

where, m, m_x, and m_y are the mass of the ship, the added mass of the entrained water in x-direction (kg) and y-direction (kg) respectively; I_z and J_z are the moment of inertia of the ship (kg·m^2) and the added moment of inertia of the entrained water (kg·m^2) respectively; v, u and r are the ship velocity in x-axis direction (m/s), ship velocity in y-axis direction (m/s) and the yaw rate around the z-axis (rad/s) respectively; $\dot{v}$, $\dot{u}$ and $\dot{r}$ are the accelerations of v, u and r respectively; X, Y and N are the external forces acting on ship in x-axis direction and y-axis direction (N) and the yaw moment around z-axis acting on ship (Nm) respectively.

The hydrodynamic forces and moments, including the wind- and waves-induced steady forces and moments, are shown in equation (2). The external forces and moments contributed by the hull, propeller and rudder components are denoted with the subscripts of H, P and R respectively.

$$\left.\begin{array}{l}X=X_H+X_P+X_R+X_A+X_W\\Y=Y_H+Y_R+Y_A+Y_W\\N=N_H+N_R+N_A+N_W\end{array}\right\} \quad (2)$$

Where, X_A, Y_A and N_A are the wind-induced steady longitudinal force, lateral force and moment respectively; X_W, Y_W and N_W are the waves-induced steady longitudinal force, lateral force and moment respectively.

The prime symbols used in the following sections refer to the non-dimensionalized quantities as follows (Kijima et al., 1990):

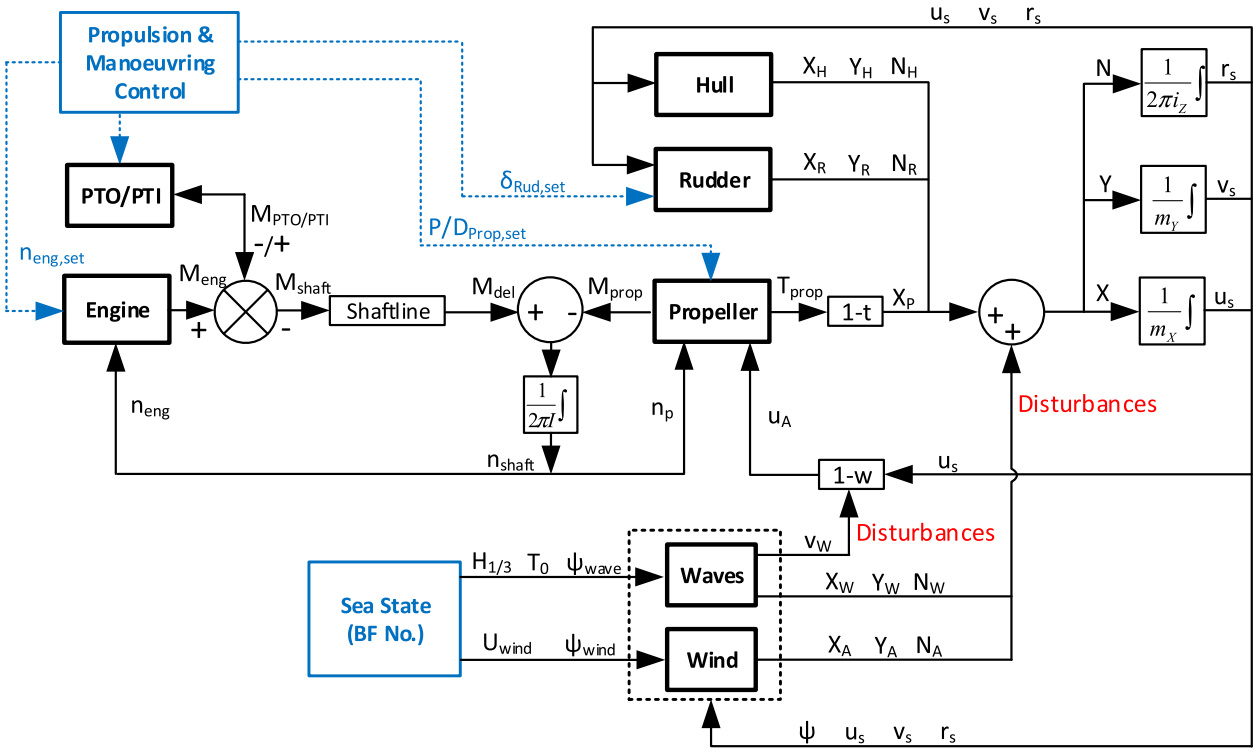

Fig. 3. Layout of integrated ship propulsion, manoeuvring and sea state model.

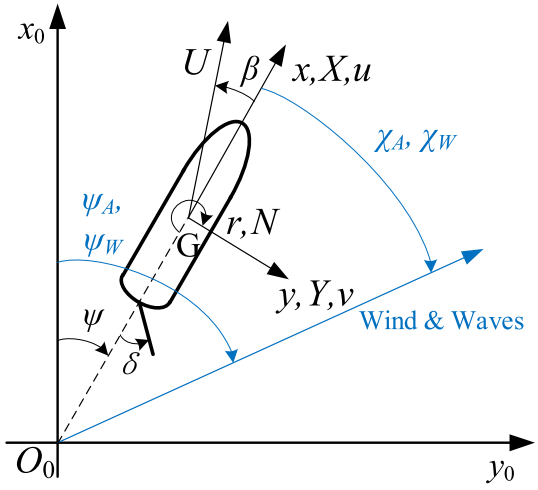

Fig. 4. Coordinate system of MMG manoeuvring model, and wind & waves.

$$\left.\begin{aligned} X',Y',N' &= \frac{X}{0.5\cdot\rho\cdot L\cdot d\cdot U^2},\frac{Y}{0.5\cdot\rho\cdot L\cdot d\cdot U^2},\frac{N}{0.5\cdot\rho\cdot L^2\cdot d\cdot U^2} \\ v',u',r' &= \frac{v}{U},\frac{u}{U},\frac{rL}{U} \end{aligned}\right\} \tag{3}$$

where, L is the length of the ship; d is the ship draught, U is the ship absolute speed ($U = \sqrt{(u^2+v^2)}$) and ρ is the water density.

3.1.1. Forces and moment by hull

The hull force in x-axis direction X_H consists of two parts, which according to (Inoue et al., 1981) are the ship resistance depending on the ship longitudinal speed u in x-axis direction (the first term in equation (4)) and the force generated by the sway and yaw motions of the ship (the second term in equation (4)).

$$X'_H = X'(u) + X'_{vr}\cdot v'\cdot r' \tag{4}$$

where, $X'(u)$ is the non-dimensional ship resistance as a function of the ship longitudinal speed u, and it is calculated using the ship resistance model introduced in (Sui et al., 2019); X'_{vr} is the hydrodynamic derivative of the coupled motions of sway and yaw in x-axis direction, which according to (Inoue et al., 1981) is calculated by equation (5).

$$X'_{vr} = (c_m - 1)\cdot m'_y \tag{5}$$

where, c_m is a constant that may have approximate values in the range of 0.5–0.75 for different ship types (Inoue et al., 1981). In (Yoshimura and Nomoto, 1978), c_m is set as 0.72–0.75 for tankers and 0.41 for container ships. In (Hasegawa, 1980) an estimation chart expressing the linear relationship between c_m and the block coefficient C_b has been proposed; a regression formula for calculating c_m, namely $c_m = 1.66\cdot C_b - 0.49$, has been made.

According to (Kijima et al., 1990), the nondimensionalized lateral force Y'_H and yaw moment N'_H acting on the ship hull are expressed by equation (6).

$$\left.\begin{aligned} Y'_H &= Y'_\beta\beta + Y'_r r' + Y'_{\beta\beta}\beta|\beta| + Y'_{rr} r'|r'| + \left(Y'_{\beta\beta r}\beta + Y'_{\beta rr} r'\right)\beta r' \\ N'_H &= N'_\beta\beta + N'_r r' + N'_{\beta\beta}\beta|\beta| + N'_{rr} r'|r'| + \left(N'_{\beta\beta r}\beta + N'_{\beta rr} r'\right)\beta r' \end{aligned}\right\} \tag{6}$$

where, Y'_β, Y'_r, …, $N'_{\beta rr}$ are hydrodynamic derivatives; X'_H, Y'_H, N'_H and r' are the nondimensionalized lateral force, yaw moment and the yaw rate of the ship respectively as shown in equation (3); β is the drift angle of the ship ($\beta = \arctan(-v/u)$).

The empirical formulas in (Kijima and Nakiri, 2003), based on a limited number of main particulars of the ship, have been used for calculating the hydrodynamic derivatives Y'_β, Y'_r, …, $N'_{\beta rr}$.

3.1.2. Force by propeller

The propeller thrust is calculated by equation (7) using the non-dimensional propeller thrust coefficient C_T^*. The four-quadrant propeller diagram, in which the thrust coefficient C_T^* is expressed versus the

hydrodynamic pitch angle β_P^* and propeller pitch ratio P/D, is developed by MARIN (the Maritime Research Institute Netherlands) for describing the entire four quadrant operation of the propeller (Klein Woud and Stapersma, 2002). The thrust coefficient C_T^* is a function of the hydrodynamic pitch angle β_P^* and the propeller pitch ratio P/D. The hydrodynamic pitch angle β_P^* is calculated by equation (8). In the manoeuvring model of the chemical tanker, the propeller model based on the four-quadrant propeller open water diagram, which has been pre-defined in a lookup table, is used to calculate the propeller thrust coefficient C_T^*. The advance speed of the propeller v_A is calculated by $v_A = u\cdot(1 - w_P)$.

$$X_P = (1-t_P)\cdot C_T^*\cdot\frac{\pi}{8}\cdot\rho\cdot D_P^2\cdot\left[v_A^2+(0.7\cdot\pi\cdot n_P\cdot D_P)^2\right] \tag{7}$$

$$\beta_P^* = \arctan\left(\frac{v_A}{0.7\pi\cdot n_P\cdot D_P}\right) \tag{8}$$

The effective wake fraction w_P generally varies during manoeuvring motions from that in the straight forward motion w_{P0} (Inoue et al., 1981). Due to the effects of the drift angle, yaw rate, ship stern shape, propeller rotation, propeller working load and even the rudder, the variation of wake fraction during manoeuvring motions is complicated (Liu, 2017). The wake factor in manoeuvring in this paper is estimated by equation (9) considering the geometrical inflow angle at the propeller position (Inoue et al., 1981; Kijima et al., 2000).

$$\left.\begin{aligned} w_P &= w_{p0}\cdot\exp\left(-4\cdot\beta_P^2\right)\\ \beta_P &= \beta - x_P'\cdot r'\\ x_P' &= -(0.5+x_G/L)\end{aligned}\right\} \tag{9}$$

where, w_{P0} is the wake factor at propeller location in straight forward motion; β_P is the geometrical inflow angle to the propeller; $x_P'(=x_P/L)$ is the relative longitudinal position of the propeller; x_G is the longitudinal distance between the centre of buoyancy and mid ship ($L_{PP}/2$), which is positive when the centre of buoyancy is forward of mid ship, while negative when backward. t_P and w_{P0} are calculated using the models introduced in (Sui et al., 2019).

3.1.3. Forces and moments by rudder

According to (Kijima et al., 2000), the rudder forces and moment X_R, Y_R and N_R are calculated by equation (10).

$$\left.\begin{aligned} X_R &= -(1-t_R)\cdot F_N\cdot\sin\delta\\ Y_R &= -(1+a_H)\cdot F_N\cdot\cos\delta\\ N_R &= -(x_R+a_H\cdot x_H)\cdot F_N\cdot\cos\delta\end{aligned}\right\} \tag{10}$$

$$F_N = 0.5\cdot\rho\cdot A_R\cdot U_R^2\cdot C_N\cdot\sin\alpha_R \tag{11}$$

$$C_N = \frac{6.13\cdot\Lambda_R}{\Lambda_R+2.25} \tag{12}$$

Where, F_N is the normal force acting on rudder; δ is rudder angle; t_R is the steering resistance deduction factor; x_R is the longitudinal position of the rudder, and it is assumed that $x_R'(=x_R/L)=x_P'$; a_H is the additional interaction coefficient (ratio of additional lateral force) indicating the interaction between rudder and hull; x_H is the longitudinal position of the additional lateral force; A_R is the rudder area; U_R is the effective rudder inflow speed; α_R is the effective rudder inflow angle; Λ_R is aspect ratio of rudder, which is commonly expressed as span/mean chord ($\Lambda_R = D_R/\overline{L}_R$), or square of the rudder span/rudder area ($\Lambda_R = D_R^2/A_R$).

The effective rudder inflow velocity U_R and the effective rudder inflow angle α_R are calculated using the methods in (Yasukawa and Yoshimura, 2015). The steering resistance deduction factor t_R, which is actually the coefficient for additional rudder drag; the rudder force increase factor a_H, which indicates the additional lateral force acting on the ship by steering due to the interaction between rudder and hull; and the non-dimensional longitudinal position x_H' ($=x_H/L$) of the addition lateral rudder force are calculated using the methods in (Kijima et al., 1990).

3.1.4. Hydrodynamic mass and moment of inertia

The ship mass m and moment of inertia I_z are calculated by equation (13).

$$\left.\begin{aligned} m &= \rho\cdot\nabla\\ I_z &= m\cdot r_{gyr}^2\end{aligned}\right\} \tag{13}$$

where, ∇ is the ship displacement volume (m^3); r_{gyr} is the gyration radius (m) ($r_{gyr} = k_{gyr}\bullet L$); k_{gyr} is the coefficient, which varies from 0.18 to 0.25 for most ships according to (Dirix, 2002), in which k_{gyr} is set as 0.225. In (Liu, 2017) k_{gyr} is set as 0.2536, while in (Yasukawa and Yoshimura, 2015) it is set as 0.25. In the model of the chemical tanker, k_{gyr} is set as 0.25.

The added mass at x-axis direction is calculated by the following formula in (Dirix, 2002).

$$m_x = \frac{m_{ship}}{\pi\sqrt{L^3/\nabla}-14} \tag{14}$$

The added mass at y-axis direction and the added moment of inertia are calculated by the following formula in (Clarke, 1983).

$$m_y = \frac{\pi}{2}\cdot\rho\cdot d^2\cdot L\cdot\left[1+0.16\cdot C_b\cdot\frac{B}{d}-5.1\cdot\left(\frac{B}{L}\right)^2\right] \tag{15}$$

$$J_z = \frac{\pi}{2}\cdot\rho\cdot d^2\cdot L^3\cdot\left(\frac{1}{12}+0.017\cdot C_b\cdot\frac{B}{d}-0.33\cdot\frac{B}{L}\right) \tag{16}$$

In the model the added masses at both x-axis and y-axis directions have been corrected by multiplying the correction factors C_{mx} (=0.5) and C_{my} (=0.5) to the results calculated by equations (14) and (15). Note that the hull form parameters used in equations (14)–(16) should be limited in an appropriate range, otherwise the mathematical calculation results of the added masses and moment of inertia of the ship could be unrealistic, for example, zero or negative. However, the determination of the appropriate ranges of the hull form parameters for different ship types is out of scope of this paper.

3.2. Wind- and waves-induced steady forces and moments

When taking the influences of wind and waves in adverse sea conditions in to account, only time-averaged steady wind- and waves-induced forces and moments acting on the ship hull will be considered, while the time-varying oscillatory forces and moments will be neglected assuming that the time scale is shorter than that of the ship motions (Shigunov, 2019).

3.2.1. Wind-induced steady forces and moment

The wind-induced external steady forces (X_A, Y_A) and moment (N_A) acting on the ship are estimated using Fujiwara's empirical wind model (Fujiwara et al., 2006; Kitamura et al., 2017). According to (Fujiwara et al., 2006) the wind forces and moment in the constant and uniform wind are expressed as:

$$\left.\begin{aligned} X_A &= 1/2\cdot\rho_a\cdot U_A^2\cdot C_{XA}(\chi_A)\cdot A_X\\ Y_A &= 1/2\cdot\rho_a\cdot U_A^2\cdot C_{YA}(\chi_A)\cdot A_Y\\ N_A &= 1/2\cdot\rho_a\cdot U_A^2\cdot C_{NA}(\chi_A)\cdot A_Y\cdot L_{OA}\end{aligned}\right\} \tag{17}$$

Where, ρ_a is the air density; U_A is the relative wind velocity; C_{XA}, C_{YA} and C_{NA} are the wind forces and moment coefficients; χ_A is the relative wind direction; A_X and A_Y are the frontal and lateral projected areas of the ship above water respectively; L_{OA} is the overall ship length.

For estimating the wind forces and moment coefficients, C_{XA}, C_{YA} and C_{NA}, when using the method in (Fujiwara et al., 2006), eight basic hull form parameters representing the above water structural shape of ships are needed. However, some of the needed above water structural parameters of the benchmark chemical tanker are not available, so, they are estimated using the regression formulae in (Kitamura et al., 2017).

3.2.2. Waves-induced steady forces and moments

According to (Yasukawa et al., 2019), the averaged waves-induced steady forces (X_W, Y_W) and moment (N_W) in irregular waves are expressed as:

$$\left.\begin{aligned} X_W &= \rho_w \cdot g \cdot H_{1/3}^2 \cdot \left(B^2/L\right) \cdot C_{XW}(U, T_v, \chi_W) \\ Y_W &= \rho_w \cdot g \cdot H_{1/3}^2 \cdot \left(B^2/L\right) \cdot C_{YW}(U, T_v, \chi_W) \\ N_W &= \rho_w \cdot g \cdot H_{1/3}^2 \cdot B^2 \cdot C_{NW}(U, T_v, \chi_W) \end{aligned}\right\} \tag{18}$$

Where, ρ_w is the sea water density; g is the gravity acceleration; $H_{1/3}$ is the significant wave height; T_v is the averaged wave period; χ_W is the relative wave direction; B and L are the ship width and length respectively; C_{XW}, C_{YW} and C_{NW} are the averaged steady forces and moment coefficients in irregular waves.

For estimating the averaged waves-induced steady forces coefficients of the benchmark chemical tanker, the numerical calculation results of those coefficients of a full hull ship S-Cb84 (Appendix Figure A. 1) published in (Yasukawa et al., 2019) have been used in this paper. The S-Cb84 is a bulk carrier, which originally was a VLCC (Very Large Crude Carrier) tanker. The principal particulars of S-Cb84 are shown in Appendix Table A. 1. The applicability of the numerical calculation results using the strip theory-based Kochin-function method (SKFM) to the manoeuvring problems in irregular waves has been validated by the free-running model test results, and it is concluded that the accuracy is acceptable for practical purposes, even though the calculation accuracy of the steady yaw moment is insufficient as mentioned in (Yasukawa et al., 2019). In the simulation model, to reduce the simulation time, the precalculated waves-induced steady forces coefficients are stored in look-up tables as functions of ship speeds, averaged wave period and wave encounter headings, as the accurate synthesis of the instantaneous value of the wave-induced steady forces is quite time-consuming (Aung and Umeda, 2020; Dallinga et al., 2020). During simulation, following the quasi-static (or quasi-steady) assumption made in (Yasukawa et al., 2019), the wave-induced steady forces coefficients in different operating conditions are estimated by using an interpolation method. Hydrodynamic forces acting on the ship are assumed quasi-steady and the high-frequency wave-induced motions and forces are neglected (Yasukawa et al., 2021; Yasukawa and Sakuno, 2020; Yasukawa and Yoshimura, 2015); the theoretical and practical reason is that, the effects of the nonzero slowly varying second-order wave-induced forces on ships and consequently on the engines are much more apparent compared to the high-frequency zero-mean oscillatory first-order wave-induced forces (Dallinga et al., 2020; Fossen and Wiley, 2011; Journee et al., 2015). Although there will be some extra uncertainties when using these numerical calculation results to a different ship, i.e., the benchmark chemical tanker used in this research, it is assumed that the uncertainties in this regard are acceptable here. The reasons for this assumption are as follows: firstly, both ships are tankers, so, they have similar hull shape although with different sizes; secondly, the numerical calculation results for the waves induced steady forces are nondimensional; thirdly, the simulation results of the benchmark chemical tanker turning in different sea states with different ship speeds have been verified (in following section), and the model verification shows reasonable results comparing to the simulation and model test results in (Yasukawa et al., 2019).

3.3. Propeller wake fluctuation in waves

The effective inflow velocity to the propeller in waves is determined by the average ship speed, ship motion and wave induced orbital motion of water particles (Ueno et al., 2013). The variation of effective wake fraction during ship manoeuvring motions in calm water considering the geometrical inflow angle at the propeller position has been discussed in section 3.1.2. According to (Ueno et al., 2013) the fluctuating propeller inflow velocities in waves are caused by the surge oscillation effect and the orbital motion of water particles. In this paper, the effect of ship manoeuvring motions on the average propeller inflow velocity and the effect of the water orbital movement on the oscillating inflow velocity in regular waves will be considered; while the effects of surge oscillation and the interaction between the ship manoeuvring motions and the water orbital movement will be left out. So, the propeller inflow velocity v_A in regular waves is expressed as:

$$v_A = u \cdot (1 - w_P) + \alpha \cdot \omega \cdot h_a \cdot \exp(-k \cdot z_P) \cdot \cos\chi_W \cdot \cos(\omega_e \cdot t - k \cdot x_P \cdot \cos\chi_W) \tag{19}$$

$$\alpha = \begin{cases} 0.2 \cdot \left(\dfrac{\lambda}{L \cdot |\cos\chi_W|}\right) + 0.5, for \dfrac{\lambda}{L \cdot |\cos\chi_W|} \le 2.5 \\ 1, for \dfrac{\lambda}{L \cdot |\cos\chi_W|} > 2.5 \end{cases} \tag{20}$$

Where, u is the ship longitudinal velocity; w_P is the effective wake fraction including the effect of ship manoeuvring motions; α is the coefficient representing the effect of wave amplitude decrease at the stern in case of head and bow-quartering waves due to the influence of the hull (calculated by equation (20)) (Ueno et al., 2013); ω is the wave circular frequency; ω_e is the wave encounter circular frequency defined by $\omega_e = \omega - k \cdot u \cdot \cos\chi_W$; h_a is the wave amplitude; k is the wave number; x_P and z_P are the longitudinal and vertical positions of the propeller in the ship-fixed coordinate system; χ_W is the wave encounter angle; t is time; λ is the wave length and L is the ship length between perpendiculars.

4. Model validation and verification

4.1. Validation of ship manoeuvring model

The integrated ship propulsion and manoeuvring model has been validated using the sea trial test data of the benchmark chemical tanker. The ship draft and environmental condition during the sea trial test have been shown in Table 4. In this paper, the sea margin (SM) is assumed to be zero (SM = 0) during the sea trial test, despite of the fact that the wind force was actually Beaufort 3–4 and the sea state was Douglas 2–3 rather than a very calm sea (Sui et al., 2019). So, when validating the ship propulsion and manoeuvring model, in the simulation model the sea margin is set at zero and the ship draft is set at design draft (8.50 m).

According to the sea trial report, only limited data of ship behaviour during sea trial test have been measured and recorded. For instance, during the deceleration and crash stop test, turning circle test and Zigzag test, only ship speed, position and heading, etc., have been measured, while the data of propeller thrust, propeller torque, ship yaw rate, drift angle, engine power and fuel rack, etc., have not been measured or recorded. So, with the limited test data the ship manoeuvring model has

Table 4
Sea trial condition of the benchmark chemical tanker.

Geographic position	East China Sea	Wind scale	3-4Bft.	Draft TF	8.50 m
Weather	Cloudy	Wind Direction	NE	Draft TM	8.55 m
Depth of Water	75 m	Sea state	Douglas 2-3	Draft TA	8.60 m

been partly validated.

4.1.1. Turning circle validation

During the turning circle sea trial test, according to the sea trial report, the engine rotational speed is kept constant at 163.7 rpm, but the propeller pitch is not recorded. However, in the simulation both the engine rotational speed and the propeller pitch are kept constant at values of 163.7 rpm and P/D = 0.6022 respectively. The ship initial speed is then 12.8 kn. For the portside turning circle test, the rudder angle is set as −35°, while for the starboard turning the rudder angle is set as 35°.

In reality the behaviour of the portside and starboard turning operations may be somewhat asymmetrical, especially for a ship with a single propeller; however, in the model all the constants are set the same for both portside steering and starboard steering. So, simulation results for portside and starboard turning are symmetrical.

To quantify the accuracy of the simulation results of the turning circle, the average relative deviation $\overline{\sigma}_T$ between the simulation results and test data are calculated as the following eq. (21):

$$\overline{\sigma}_T = 100\% \times \left(\left| \frac{x_{0\max}^{Sim} - x_{0\max}^{Test}}{x_{0\max}^{Test}} \right| + \left| \frac{y_{0\max}^{Sim} - y_{0\max}^{Test}}{y_{0\max}^{Test}} \right| + \left| \frac{R_C^{Sim} - R_C^{Test}}{R_C^{Test}} \right| + \left| \frac{V_C^{Sim} - V_C^{Test}}{V_C^{Test}} \right| \right) \Big/ 4 \tag{21}$$

Where, $x_{0\max}$ is the maximum advance (m); $y_{0\max}$ is the maximum transfer (m); R_C is the steady turning radius (m); V_C is the ship speed in steady turn (kn). The maximum advance $x_{0\max}$, maximum transfer $y_{0\max}$ and the steady turning radius R_C are defined and illustrated in Fig. 5 (ITTC, 2017).

4.1.1.1. Portside turning. The validation results of the portside turning circle test with a rudder angle of −35° are shown in Fig. 6 and Table 5. The average relative deviation $\overline{\sigma}_T$ between the simulation results and the sea trial test data of the portside turning circle is 7.70%. The uncertainties of the validation results will be analysed later in the following section.

4.1.1.2. Starboard turning. The validation results of the starboard turning circle test with a rudder angle of 35° are shown in Fig. 7 and Table 6. The average relative deviation $\overline{\sigma}_T$ between the simulation results and the sea trial test data of the starboard turning circle is 8.18%. The uncertainties of the validation results will be analysed later in the following section.

4.1.2. Zigzag validation

During the Zigzag test, the engine rotational speed is kept constant while the propeller pitch is unknown. However, in the simulation of Zigzag operation both the engine speed and the propeller pitch are set at constant values of 163.7 rpm and P/D = 0.5661 respectively. The ship initial speed is then 12.3 knots, which is according to the sea trial test

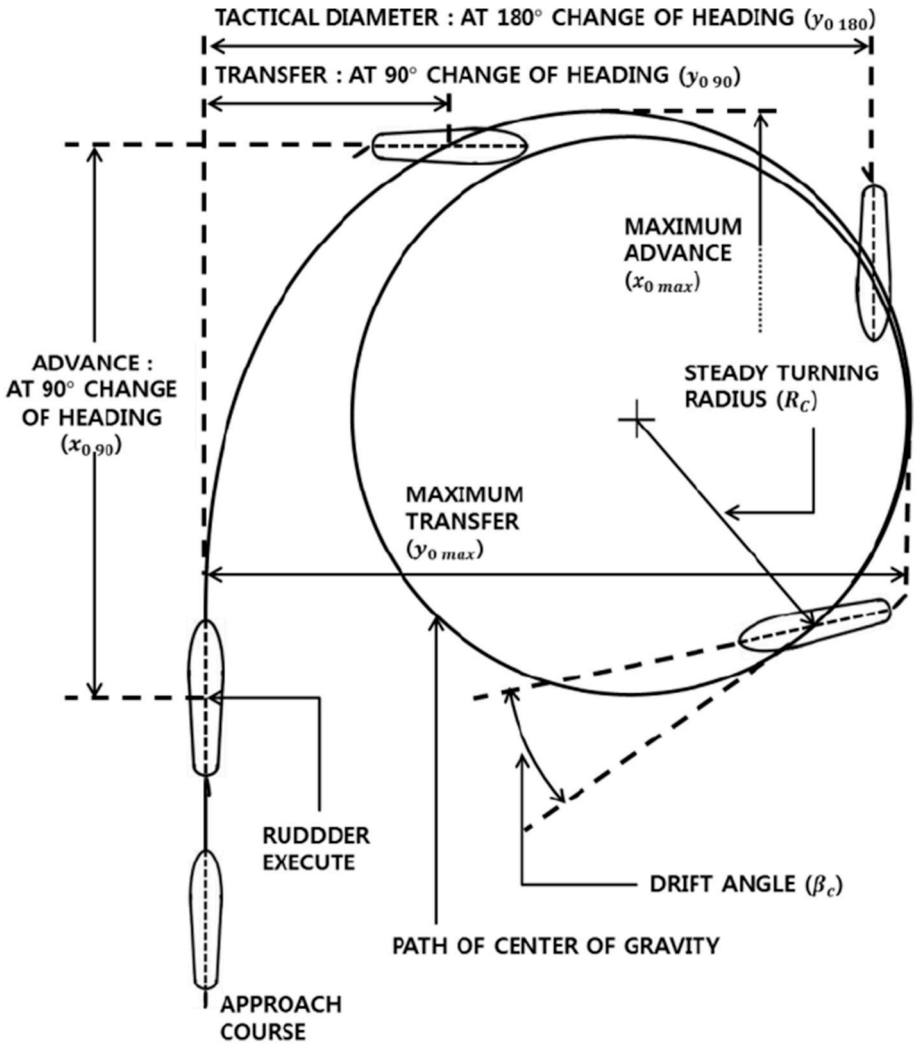

Fig. 5. Turning circle definitions (ITTC, 2017).

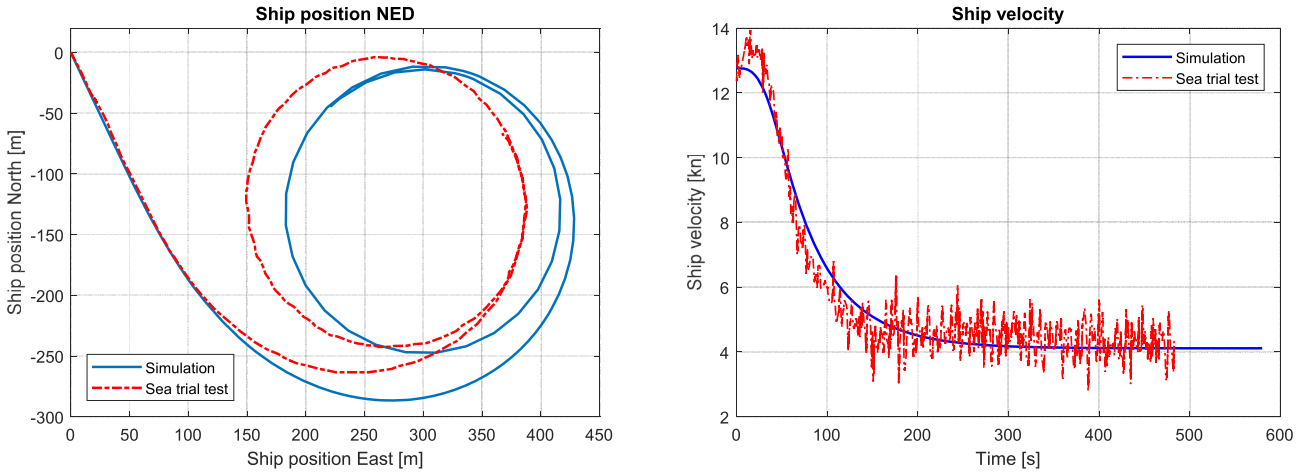

(a) Ship position in NED system (b) Ship velocity - time

Fig. 6. Validation results of turning circle trial (Portside with rudder angle: 35 deg.).

Table 5
Deviation between simulation results and test data of turning circle(Portside with rudder angle: 35 deg.).

Turning Criteria	Test	Sim.	Relative Deviation σ_T (%)	Average Relative Deviation $\overline{\sigma}_T$ (%)
x_{0max} (m)	358.60	392.50	9.45	7.70
y_{0max} (m)	304.10	335.40	10.29	
R_C (m)	120.40	116.25	3.45	
V_C (kn)	4.47	4.13	7.61	

data.

To quantify the accuracy of the simulation results of the Zigzag test, the average relative deviation $\overline{\sigma}_Z$ between the simulation results and test data are calculated as the following eq. (22) (Liu, 2017):

$$\overline{\sigma}_Z = 100\% \times \left(\left| \frac{\psi_{O1}^{Sim} - \psi_{O1}^{Test}}{\psi_{O1}^{Test}} \right| + \left| \frac{\psi_{O2}^{Sim} - \psi_{O2}^{Test}}{\psi_{O2}^{Test}} \right| + \left| \frac{t_{O1}^{Sim} - t_{O1}^{Test}}{t_{O1}^{Test}} \right| + \left| \frac{t_{O2}^{Sim} - t_{O2}^{Test}}{t_{O2}^{Test}} \right| \right) \Big/ 4 \tag{22}$$

Where, ψ_{O1} is the first overshoot angle (deg.) at time t_{O1} (s); ψ_{O2} is the second overshoot angle (deg.) at time t_{O2} (s) (defined and illustrated in Fig. 8).

4.1.2.1. Rudder: 10 deg. The validation results of the Zigzag operation with rudder angle of 10° are shown in Fig. 9(a) and Table 7. The data of ship velocity during Zigzag tests has not been recorded in the sea trial report, so, the test data of ship velocity is not available for validating the simulation results. A clear inconsistency between the simulation results and the sea trial data is shown (Fig. 9 (a)) and the average relative deviation $\overline{\sigma}_Z$ is 23.25% (Table 7). The uncertainties of the validation results will be analysed later in the following section.

4.1.2.2. Rudder: 20 deg. The validation results of the Zigzag test with rudder angle of 20° are shown in Fig. 10(a) and Table 8. A good consistency between the simulations results and the sea trial data is shown and the average relative deviation $\overline{\sigma}_Z$ is 2.19%.

Table 6
Deviation between simulation results and test data of turning circle(Starboard with rudder angle: 35 deg.).

Turning Criteria	Test	Sim.	Relative Deviation σ_T (%)	Average Relative Deviation $\overline{\sigma}_T$ (%)
x_{0max} (m)	368.40	392.50	6.54	8.18
y_{0max} (m)	300.00	335.40	11.80	
R_C (m)	123.85	116.25	6.14	
V_C (kn)	4.50	4.13	8.22	

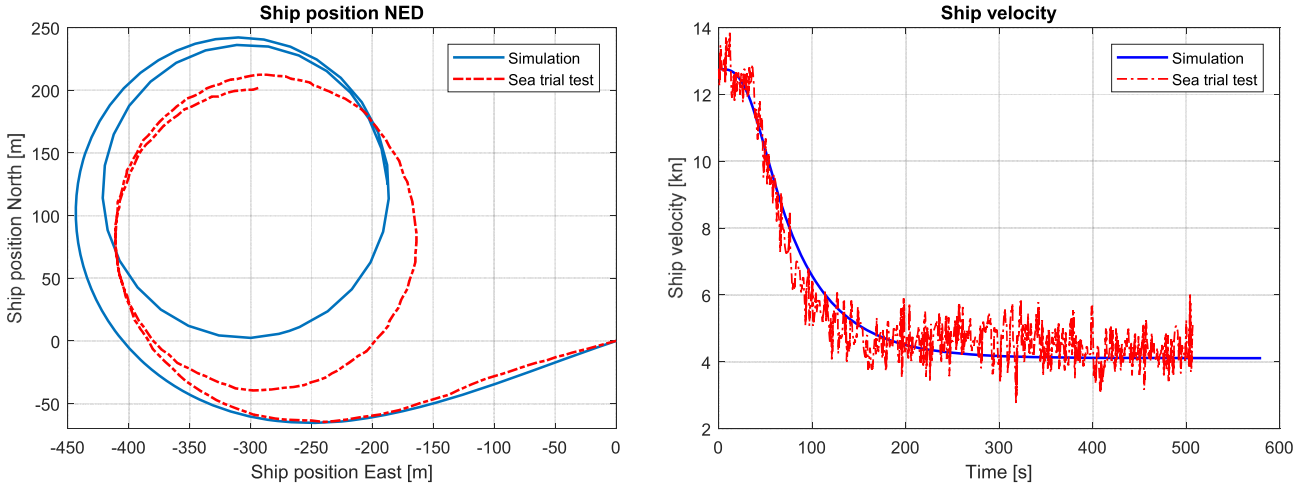

(a) Ship position in NED system (b) Ship velocity - time

Fig. 7. Validation results of turning circle trial (Starboard with rudder angle: 35 deg.).

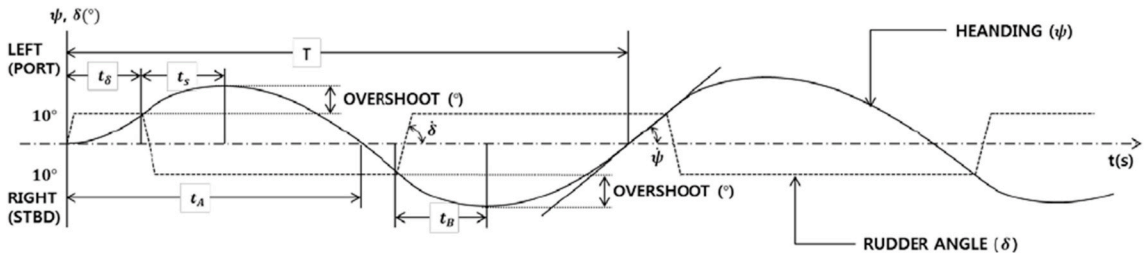

Fig. 8. Time trace of Zigzag manoeuvre parameters (ITTC, 2017).

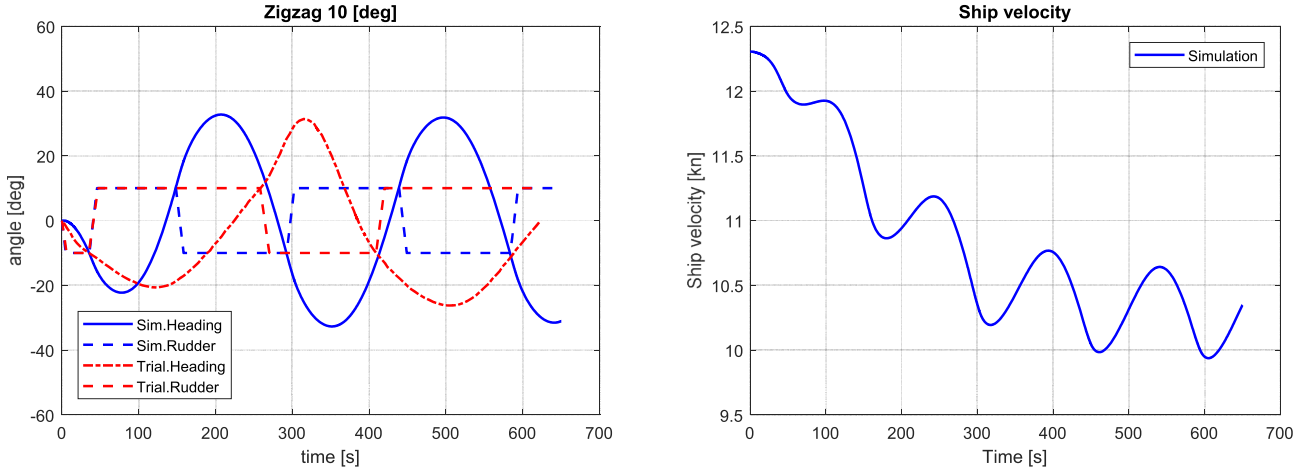

(a) Ship heading and rudder angle (b) Ship velocity - time

Fig. 9. Validation results of Zigzag test (Rudder angle: 10 deg.).

Table 7
Deviation between simulation results and test data of Zigzag(Zigzag with rudder angle: 10 deg.).

Turning Criteria	Test	Sim.	Relative Deviation σ_Z (%)	Average Relative Deviation $\bar{\sigma}_Z$ (%)
ψ_{O1} (deg.)	10.65	12.27	15.21	23.25
ψ_{O2} (deg.)	21.37	22.73	6.36	
t_{O1} (s)	124.10	78.00	37.15	
t_{O2} (s)	315.10	207.10	34.27	

Table 8
Deviation between simulation results and test data of Zigzag(Zigzag with rudder angle: 20 deg.).

Turning Criteria	Test	Sim.	Relative Deviation σ_Z (%)	Average Relative Deviation $\bar{\sigma}_Z$ (%)
ψ_{O1} (deg.)	24.59	24.88	1.18	2.19
ψ_{O2} (deg.)	24.92	25.11	0.76	
t_{O1} (s)	77.32	82.05	6.12	
t_{O2} (s)	204.60	206.00	0.68	

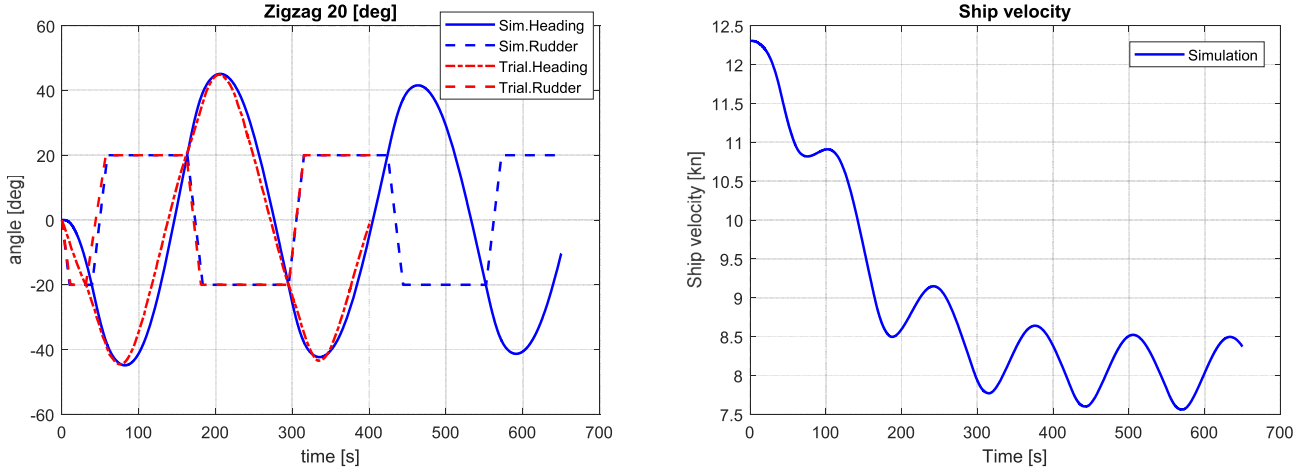

(a) Ship heading and rudder angle (b) Ship velocity - time

Fig. 10. Validation results of Zigzag test (Rudder angle: 20 deg.).

4.1.3. Uncertainty analysis

From the validation results shown above, differences between the simulation results and the sea trial test data have been found. The uncertainties causing the differences could exist in the model, the simulation process, and also the sea trial test data.

In the manoeuvring model, some hydrodynamic coefficients for calculating the manoeuvring forces and moments are calculated (using empirical formulas) or estimated as constants, while in reality they could change due to the changes of ship motions and rudder angles. As mentioned in (Sui et al., 2021), the applied propeller model is based on the corrected open water characteristics of Wageningen C4-55 propeller rather than the real propeller that is installed in the benchmark chemical tanker. Although the data of C4-55 open water characteristics has been corrected based on the data of the real propeller at design pitch in the first quadrant, there are still uncertainties in the propeller model at off-design pitches as well as in the other operating quadrants.

Uncertainties could also exist in the sea trial test data. For instance, the sea trial data of Zigzag with rudder angle of 10° is somewhat questionable or wrong. The larger rudder angle (20 deg.) Zigzag test has shown a logical, stable and symmetrical behaviour. A similarly stable behaviour is expected when the excitation is less, i.e., a smaller rudder angle (10 deg.). The ship behaviour with smaller rudder angle (10 deg.) to portside is different when moving to starboard, the rotation in one direction takes longer and changes much slower than in the other direction. However, even unstable ships should have a more or less symmetrical response to the same input signal, i.e., the rudder angle. Although in general the oscillation periods of ship heading of Zigzag with smaller rudder angle are longer, the sea trial test data of this benchmark ship has shown a much longer period of Zigzag with rudder angle of 10° than that of 20° when comparing it with the results from literature (Aoki et al., 2006; Kijima and Nakiri, 2002; Liu, 2017; Yasukawa and Yoshimura, 2015; Zaky et al., 2018).

4.2. Verification of wind and waves model

As there are no test data for validating the wind and waves model of the benchmark chemical tanker, only verification results of the ship turning in wind and waves are provided as shown in Fig. 11. The average waves period of 8 s (T_y = 8 s) has been applied. The ship turning trajectories, including both starboard and portside turning with rudder angle of 35°, in sea states of BF6 and BF7 have been compared with those in calm sea (BF0). The influences of different initial ship speed, i.e., 12 knots, 8 knots and 4 knots, on turning in wind and waves have also been presented. During turning, the propeller pitch is set and kept at the design pitch (pitch angle = 17.83° or equivalently P/D = 0.7075), and the propeller rotational speed is set and kept at the MCR engine rotational speed (167 rpm). The ship velocities during the turning are shown in Fig. 12. According to the results shown in Fig. 11, the ship drifts more significantly in higher sea state and in the same sea state the ship drifts more significantly with a lower ship speed. It is caused by the relatively large effect of the wave-induced steady forces on the ship when turning with a lower speed and/or in a higher sea state (Yasukawa et al., 2019).

5. Results and discussions

5.1. Ship propulsion and manoeuvring performance in adverse sea

In this section, based on the integrated ship propulsion, manoeuvring and sea state model, the ship propulsion and manoeuvring performance of the benchmark chemical tanker in adverse sea conditions (sea states of BF7 and BF8) will be investigated. In particular, the two most important scenarios when the ship operates in adverse sea, i.e., sailing in head sea and turning to head sea, will be studied in details. So, the abilities of the ship to keep a certain advance speed, and to keep and change heading in adverse sea will be investigated. During the simulation of the ship sailing and manoeuvring in adverse sea, the shaft generator (PTO) has been shut off, so the main engine only provides power to the propeller and the onboard electric power is supplied by the auxiliary generators. As fixed pitch propellers are most commonly installed on ocean-going cargo ships, to have a generic study, the constant pitch propulsion control mode has been applied in this investigation. The propeller pitch is set and kept at the design pitch (pitch angle = 17.83° or equivalently P/D = 0.7075). So, the ship speed will be controlled by changing the propeller rotational speed and thus the engine speed setpoint. The fuel rack limiter of the engine is switched on so that the engine can only run inside its specified operating envelope and it will not be mechanically overloaded.

5.1.1. Ship sailing in head sea

The ship heads to North (ψ = 0 deg.) and the head wind and waves come from the North ($\psi_A = \psi_W$ = 180 deg.). The rudder angle is set and kept at zero degree. The propeller rotational speed is set and kept at the MCR engine value (167 rpm) as shown in Fig. 13. The simulation results of the ship sailing in head sea are shown in Figs. 13–17.

Due to the wake fluctuation caused by the waves, the propeller advance speed and advance coefficient fluctuates and consequently the

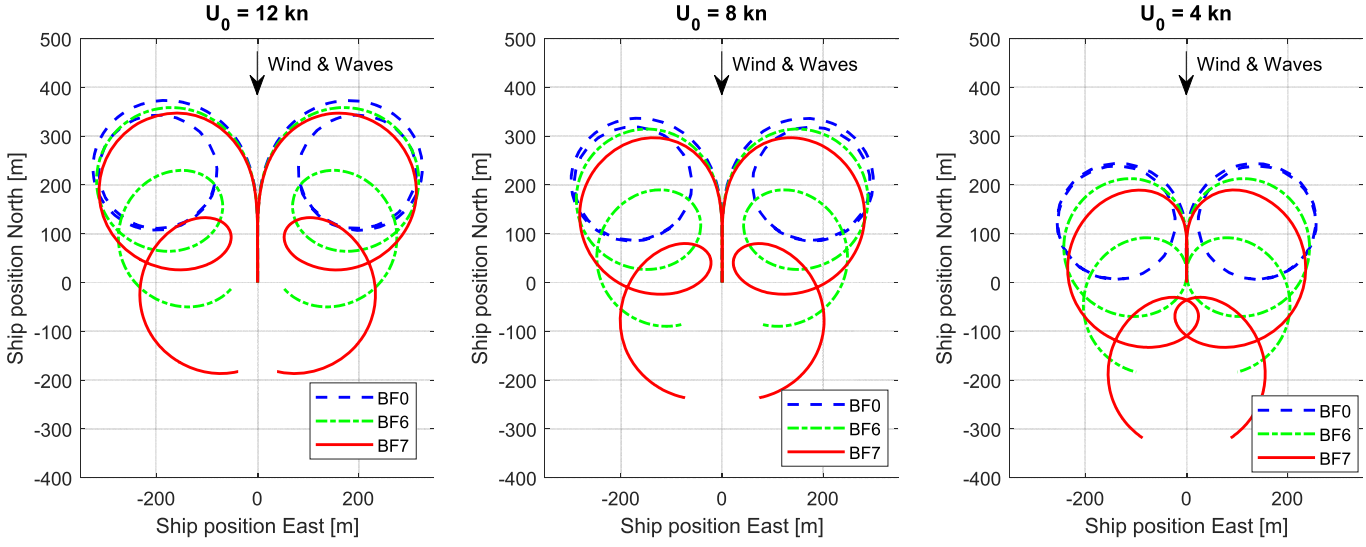

Fig. 11. Ship turning trajectories in wind and waves (rudder angle: 35 deg.).

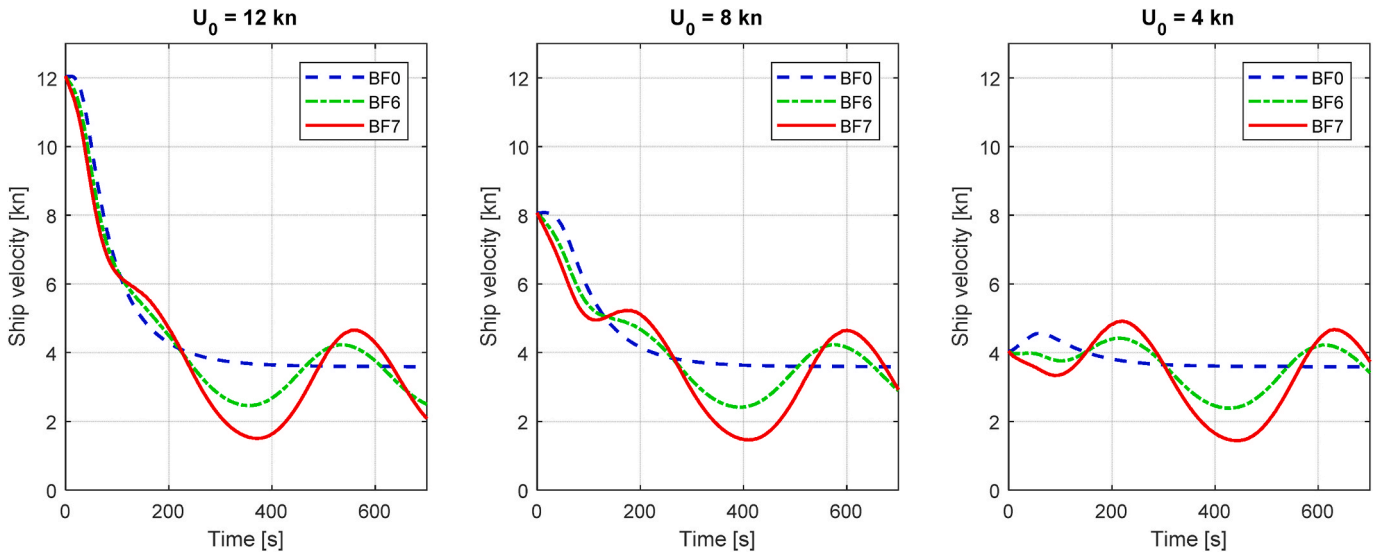

Fig. 12. Ship velocity during turning in wind and waves (rudder angle: 35 deg.).

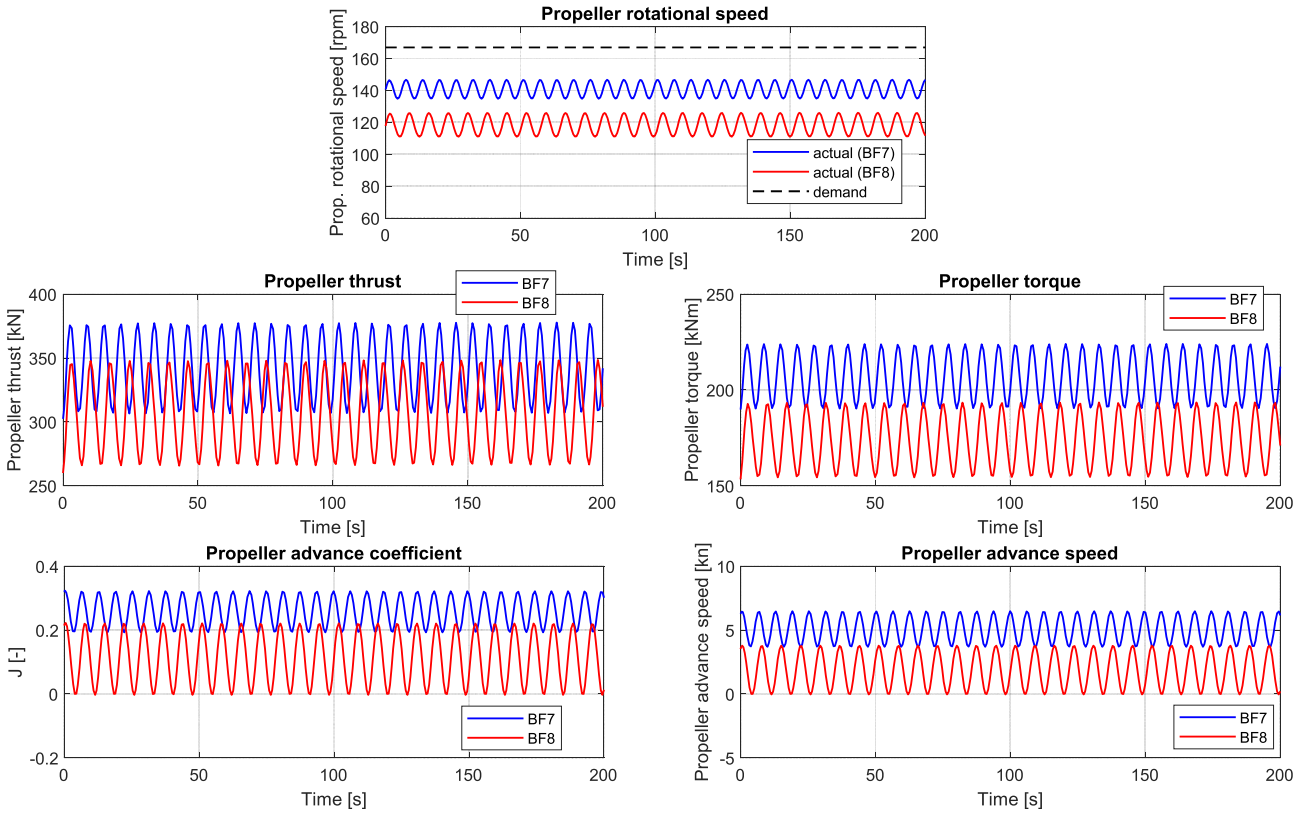

Fig. 13. Propeller rotational speed, propeller thrust, propeller torque, propeller advance coefficient, propeller advance speed when ship sails in head sea.

propeller torque, thrust and rotational speed also oscillates (Fig. 13). However, the ship velocity hardly fluctuates due to the big inertia of the ship surge motion. The maximum available ship thrust in different sea conditions oscillates around the static thrust limit as shown in Fig. 14, and the equilibrium point of the oscillation locates on the static thrust limit. So, the waves-induced wake fluctuation and the resulting ship thrust fluctuation on average do not have an influence on the ship speed. But the ship speed is highly influenced by the added ship resistance in adverse sea. The maximum ship advance speed sailing in head sea of BF7 is 7.0 knots, while in head sea of BF8 the maximum speed is only 2.6 knots. In head sea of BF9, the ship is not able to move forward at all as the ship resistance completely exceeds the ship thrust limit (Fig. 14).

The engine behaviour also fluctuates because of the fluctuating loads, i.e., the propeller torque (Fig. 15 to Fig. 17). The engine is not able to run at the demanded rotational speed because the fuel rack and consequently the engine torque are limited to protect the engine from overloading as shown in Fig. 15. The engine runs on its limit but still not exceeding the (static) operating envelope. However, dynamically the engine could have already been thermally overloaded especially in BF8 sea condition as shown in Fig. 16. The air excess ratio and the cylinder temperature just before EO exceeds their limits in sea state of BF8. Remarkably the estimated exhaust valve temperature and the

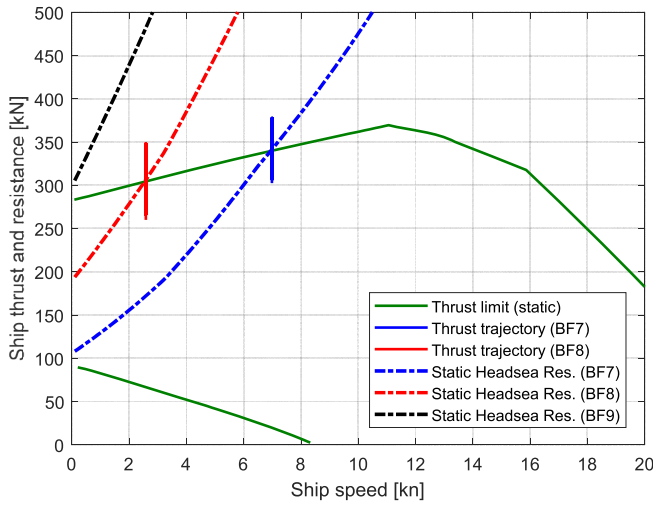

Fig. 14. Ship thrust and resistance when sailing in head sea.

temperature before turbine in the exhaust receiver seem to be lower for BF8 than for BF7. In (Sui et al., 2021) it was already observed that the large slip factor of two-stroke diesel engines helps cooling the exhaust valve temperature and the temperature in the outlet receiver before the turbine. So, it may perhaps be concluded that the exhaust valve and turbine inlet blades may be not critical when it comes to thermal overloading in heavy weather. Without reducing the propeller pitch, the engine is forced to operate at low-speed area in adverse sea condition, and this is the case for most of the ocean-going cargo ships that have fixed pitch propeller. In particular, the engine speed in BF8 is lower than that in BF7, and consequently the turbocharger speed, the charging pressure and the air mass flow in BF8 are lower as well. Although the compressor does not surge in both BF7 and BF8, the compressor operating point in BF8 is closer to the surge line than that in BF7.

The determining factor for the limit thrust is from right to left the maximum engine rotational speed, power, torque and then the air limit and finally (appearing at the bottom) the minimum engine rotational speed.

5.1.2. *Ship turning to head sea*

The initial ship forward speed is set at $u = 6.5$ knots and the initial ship heading is set at $\psi = 0°$ (heading towards North) (see Fig. 22). The wind and waves come from West ($\psi_A = \psi_W = 90°$) towards the portside of the ship. The ship tries to turn its bow to head wind and waves for weather-vanning. Same as sailing in head sea, during ship turning to head sea the propeller rotational speed is set and kept at the MCR engine speed (167 rpm). In the simulation the ship heading is controlled in autopilot mode, where the rudder angle is controlled by a PID heading controller based on the demanded ship heading and actual heading feedback. The simulation results of ship turning to head sea are shown in Fig. 18 to Fig. 23.

According to the simulation results, the ship is able to turn its bow to head sea in both sea states of BF7 and BF8, while in BF9 the ship is not able to make it before the forward speed drops to zero as shown in Fig. 18 (a). Note that the ship initial forward speed has an influence on the ship turning behaviour. If the ship speed is too slow, the ship will not be able to turn its bow to head waves even in sea state of BF7. Although the ship with initial speed of 6.5 knots is able to turn to head waves in BF8, it cannot make it with a lower speed, for instance 2.6 knots, which is the maximum speed the ship can reach in head sea condition in BF8.

When the turning to head sea starts, the propeller rotational speed, thrust and torque will increase from the initial values (Fig. 19), while the ship longitudinal velocity will drop due to the dominating increasing ship resistance (Fig. 20). Both the engine mechanical and thermal loads will increase during ship turning to head sea (Fig. 21 to Fig. 23), and while the engine, due to the fuel rack limiter the engine is not

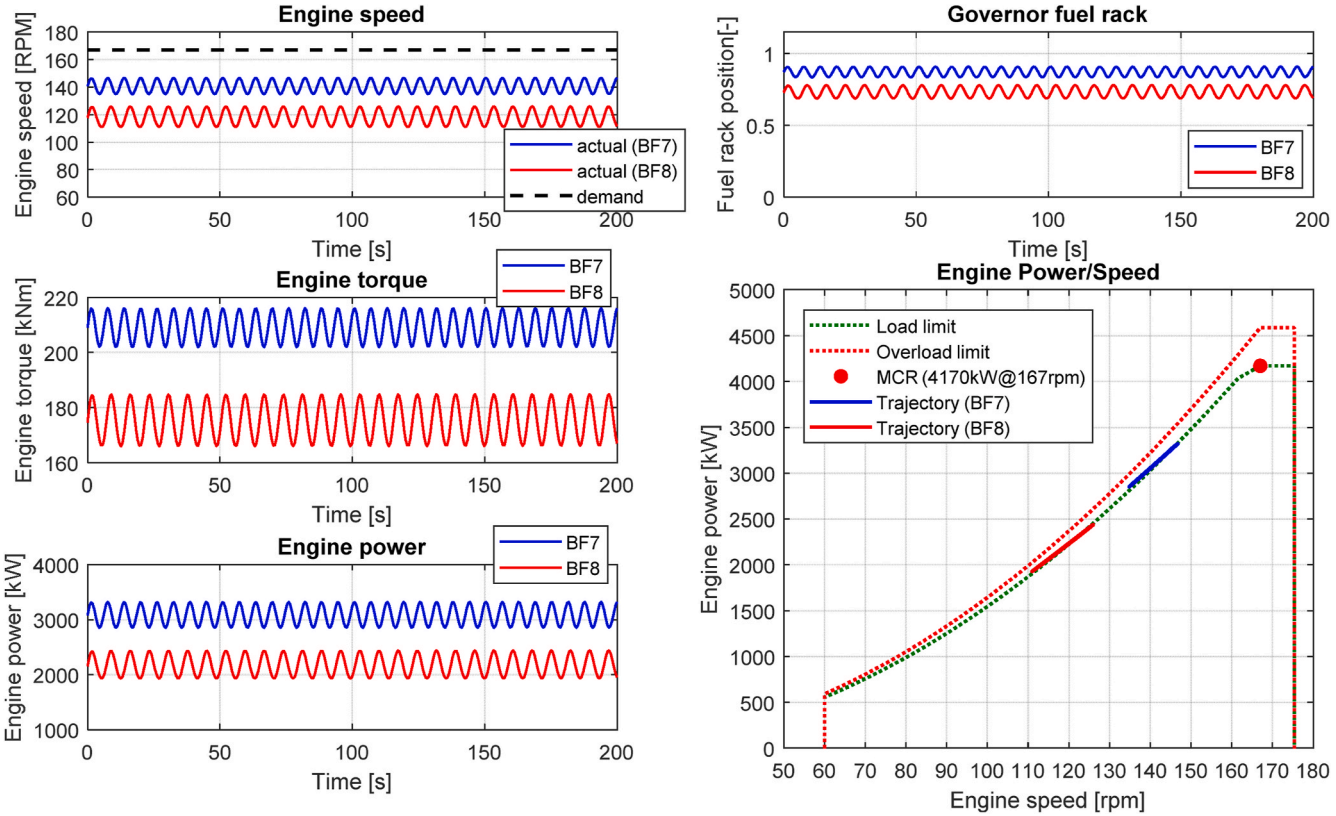

Fig. 15. Engine speed, fuel rack, torque and power when ship sails in head sea.

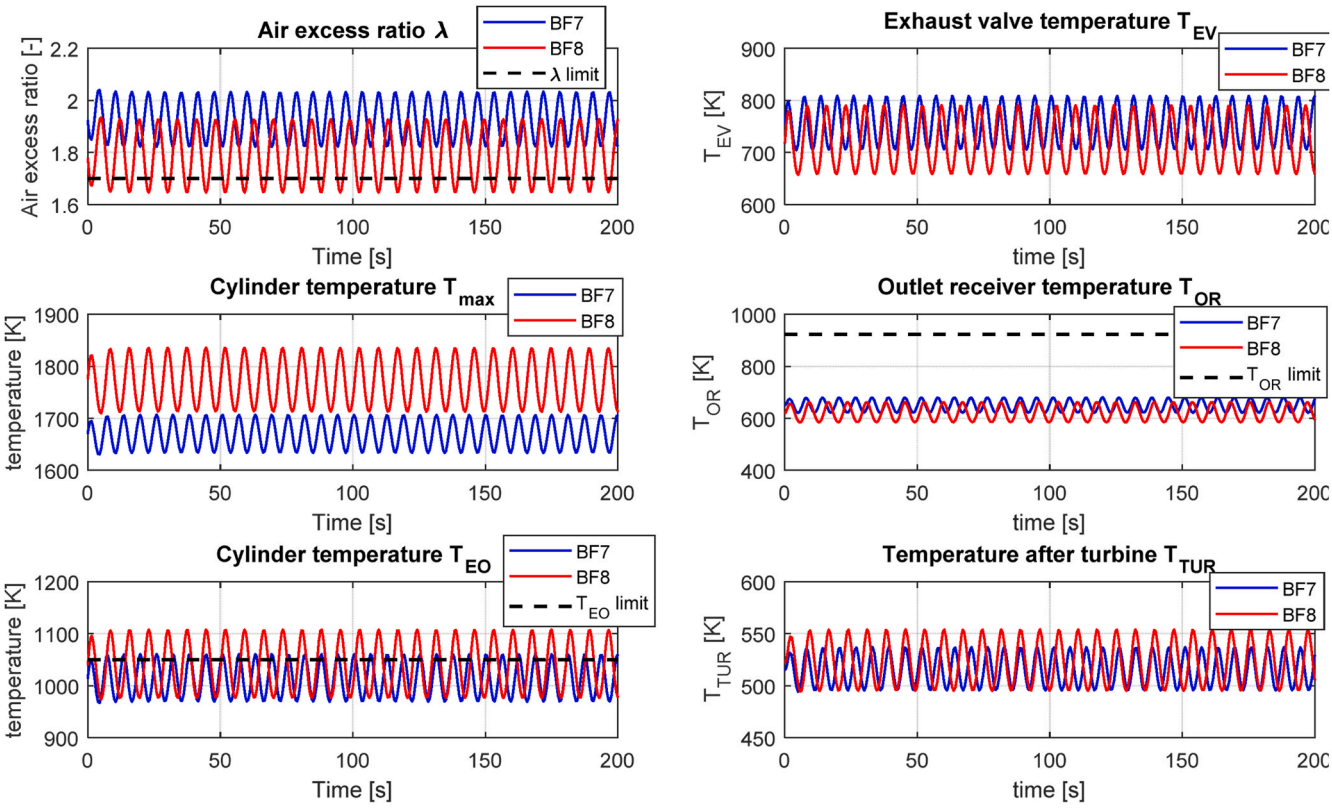

Fig. 16. Air excess ratio, exhaust valve temperature, maximum in-cylinder temperature, outlet receiver temperature, in-cylinder temperature just before EO and turbine outlet temperature when ship sails in head sea.

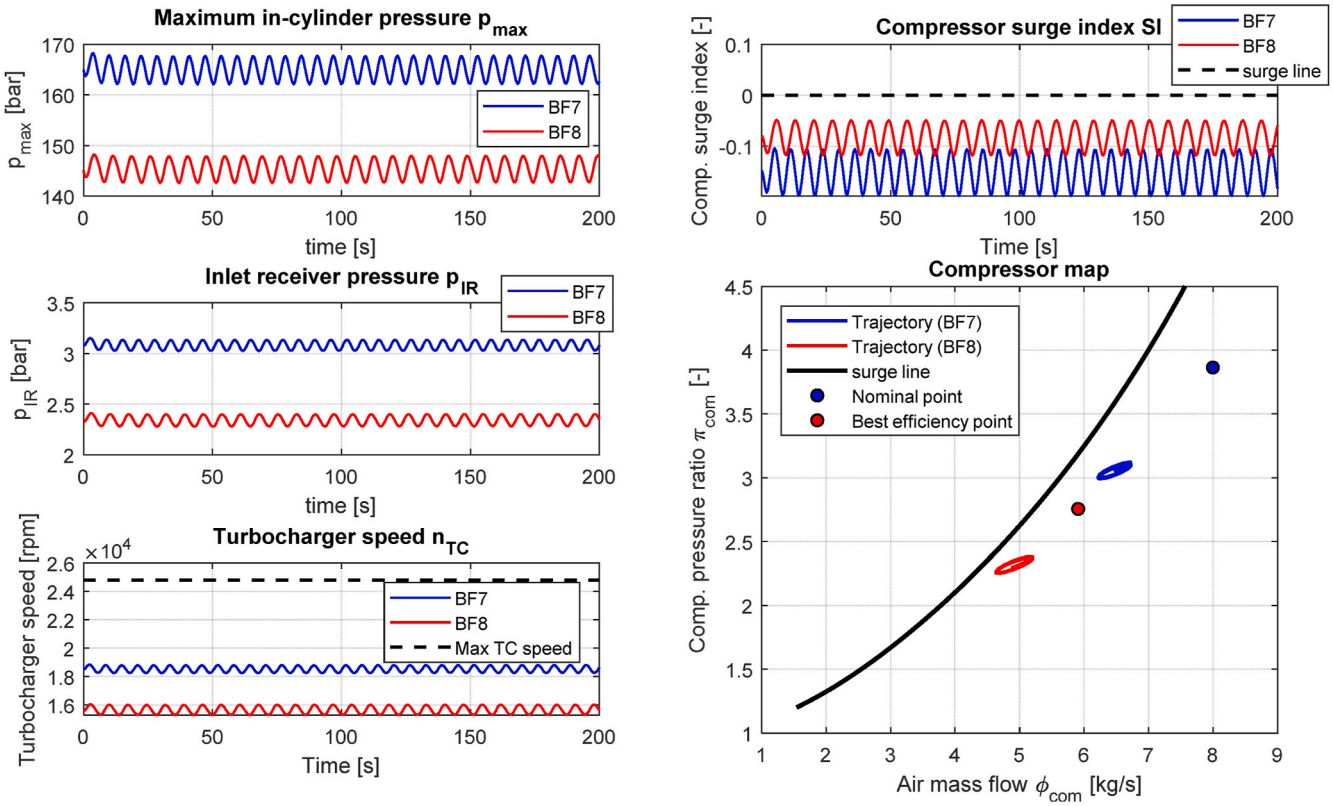

Fig. 17. Maximum in-cylinder pressure, inlet receiver pressure, turbocharger rotational speed, compressor surge index and compressor behaviour when ship sails in head sea.

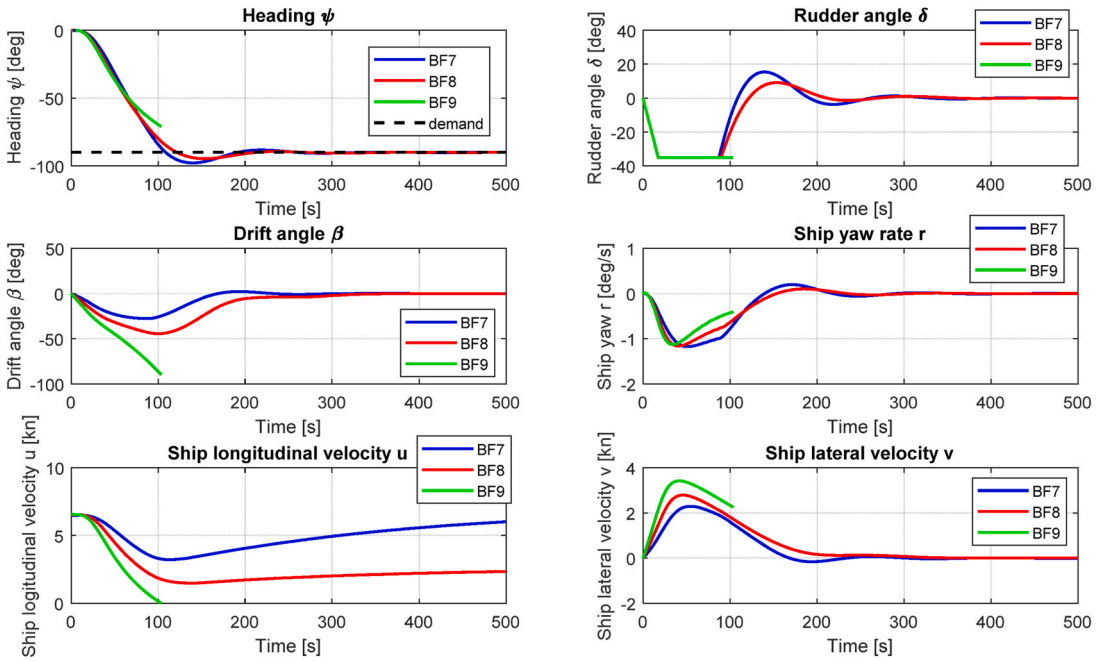

(a) Ship heading, rudder angle, drift angle, yaw rate, ship longitudinal velocity and ship lateral velocity during ship turning to head sea

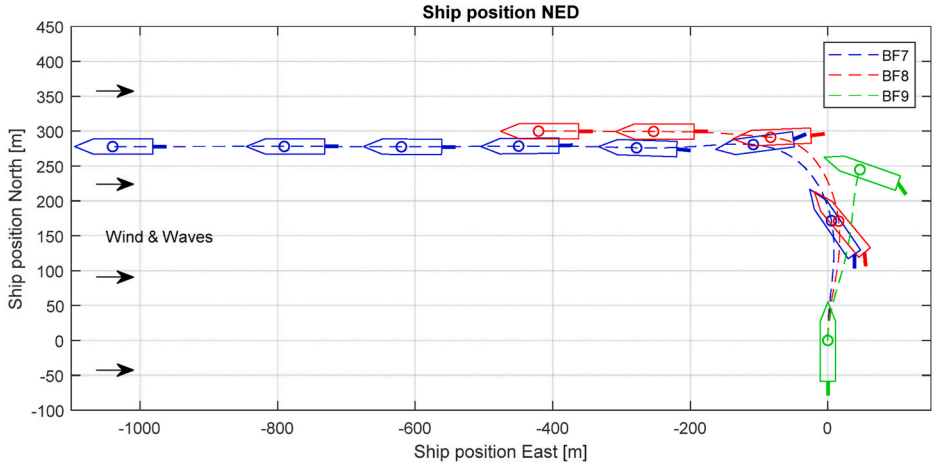

(b) Ship position trajectory during turning to head sea

Fig. 18. Simulation results of ship during turning to head sea.

mechanically overloaded, it is thermally overloaded especially in BF8, at least considering the air excess ratio and in cylinder temperatures, but again the exhaust valve temperature and outlet receiver temperature are less affected. When the ship has turned its bow to head waves, the ship velocity will increase again trying to accelerate slowly in head sea. The propeller load and engine load will drop slightly and increase again slowly until reaching a stable condition sailing in head waves, which has been discussed in previous section.

5.2. Influence of operational measures

5.2.1. Influence of propeller pitch

For a controllable pitch propeller, the ship thrust limit will be different at different propeller pitches even if for the same engine power limit (Fig. 24). The ship thrust envelopes with propeller pitches of 60%, 80% and 100% of the design pitch have been shown in Fig. 24. When the ship is sailing in adverse weather conditions, due to the significant ship resistance increase caused by the wind and waves, the ship resistance curves will shift to the upper left side of the ship thrust envelope (Fig. 24). In sea state of BF9, the ship head sea resistance is completely outside the thrust envelope when 100% design pitch has been applied. Taking sea state of BF8 for instance, in order to sail the ship at sustained speed of 5 knots without overloading the engine, the propeller pitch should be reduced accordingly to 80% design pitch, otherwise the ship can only sail at a maximum velocity of 2.6 knots. When the propeller pitch has been reduced, the engine can consequently run at a higher speed, which helps to reduce the engine thermal loading (Fig. 25). However, reducing the propeller pitch should be careful, otherwise the engine could be more likely to encounter over-speeding, which could cause the engine shutting down.

5.2.2. Influence of power-take-in (PTI)

If the main engine also provides power to a shaft generator (PTO, power-take-off), the ship thrust envelope will become smaller; while the thrust envelope will be enlarged if a shaft motor (if any) (PTI, power-take-in) also provides power to the propeller (Fig. 26). The ship thrust

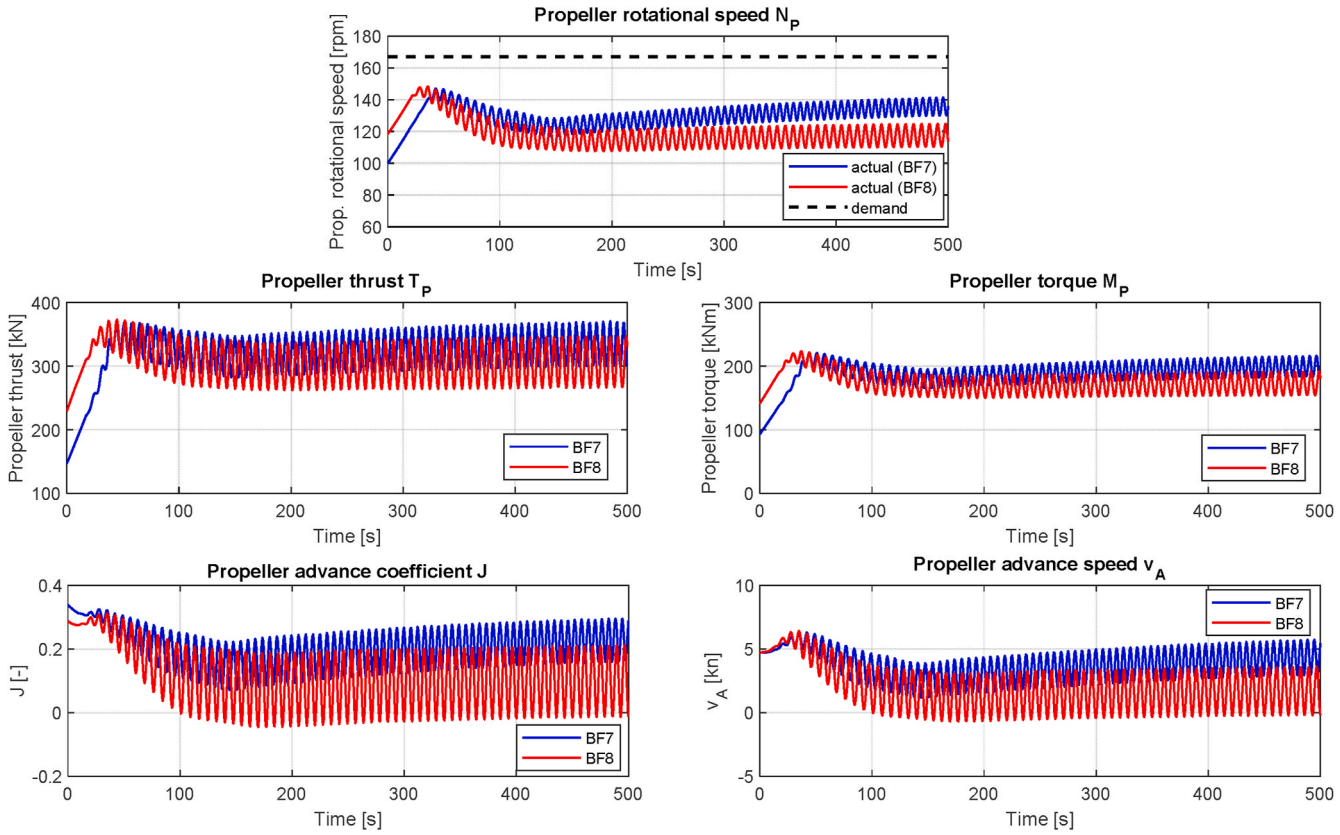

Fig. 19. Propeller rotational speed, propeller thrust, propeller torque, propeller advance coefficient, propeller advance speed during ship turning to head sea.

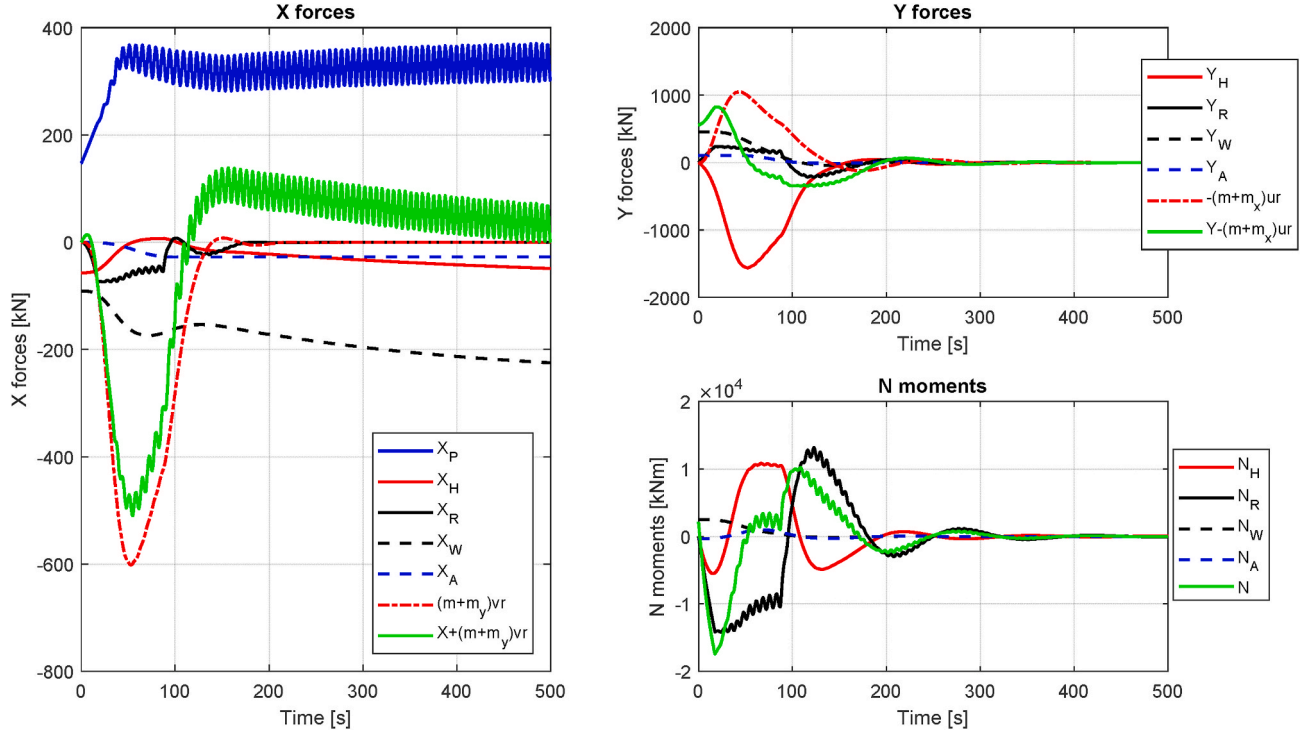

Fig. 20. Hydrodynamic forces and moments during ship turning to head sea in BF7.

envelope with PTO power of 350 kW, and PTI power of 500 kW and 1000 kW are shown in Fig. 26. Taking sea state of BF8 for instance, with a PTI power of 1000 kW, the ship is able to sail at a maximum speed of 6 knots (at design propeller pitch) in head sea condition, otherwise the ship can only sail at a maximum speed of 2.6 knots without PTI. The operation of PTI also helps to increase the engine operating speed and

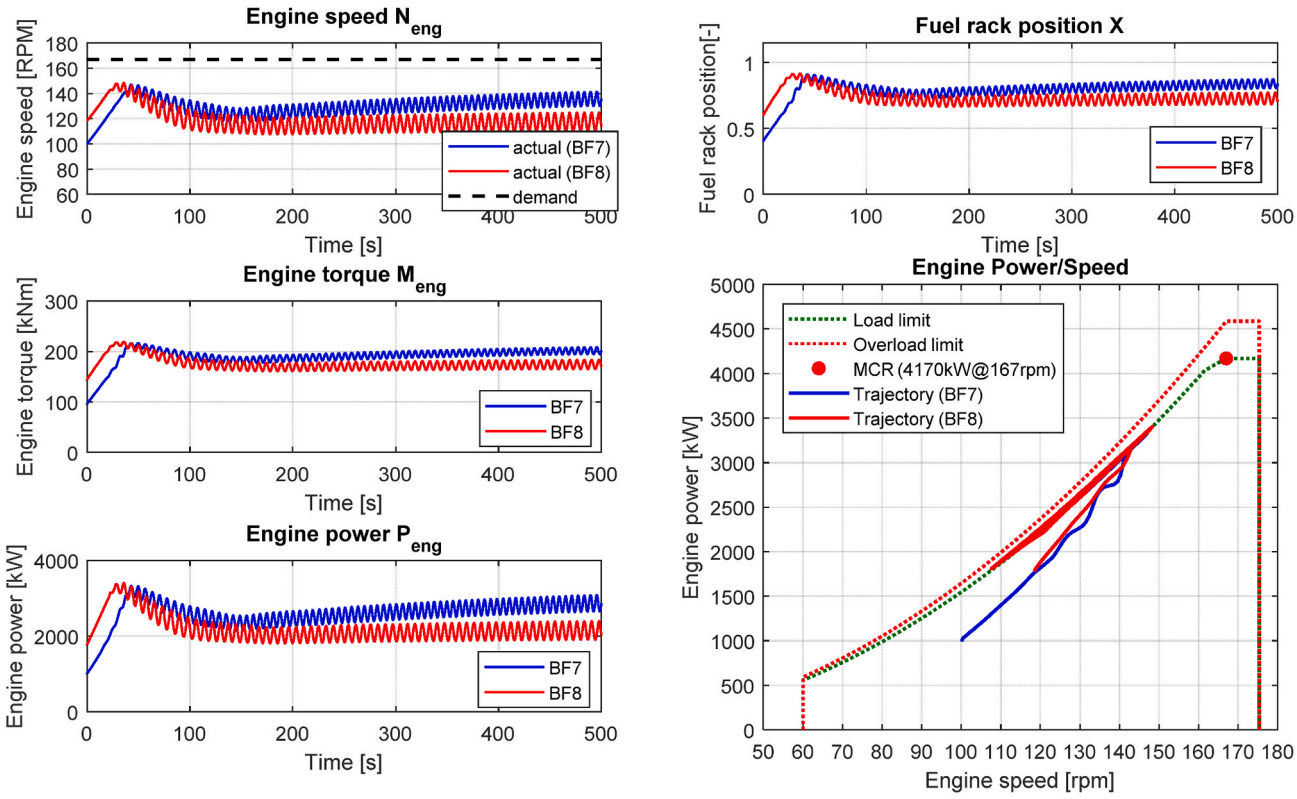

Fig. 21. Engine speed, fuel rack, torque and power during ship turning to head sea.

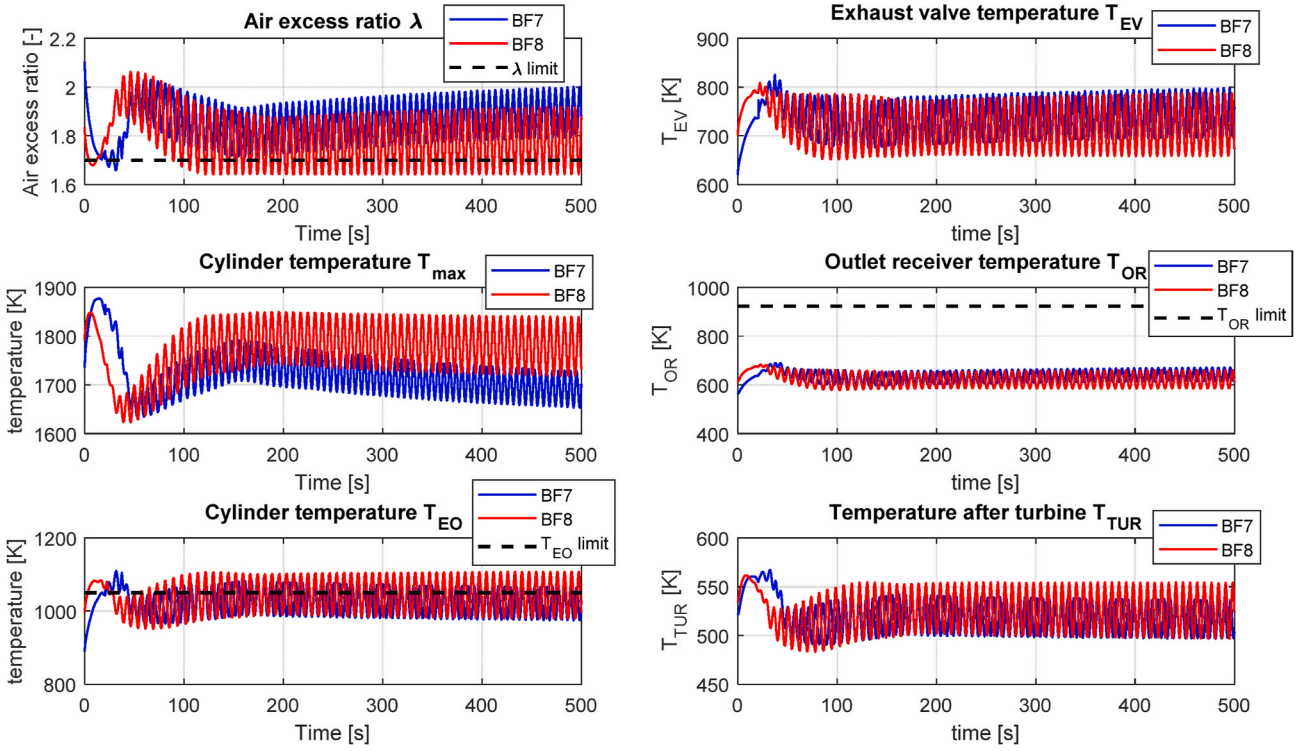

Fig. 22. Air excess ratio, exhaust valve temperature, maximum in-cylinder temperature, outlet receiver temperature, in-cylinder temperature just before EO and turbine outlet temperature during ship turning to head sea.

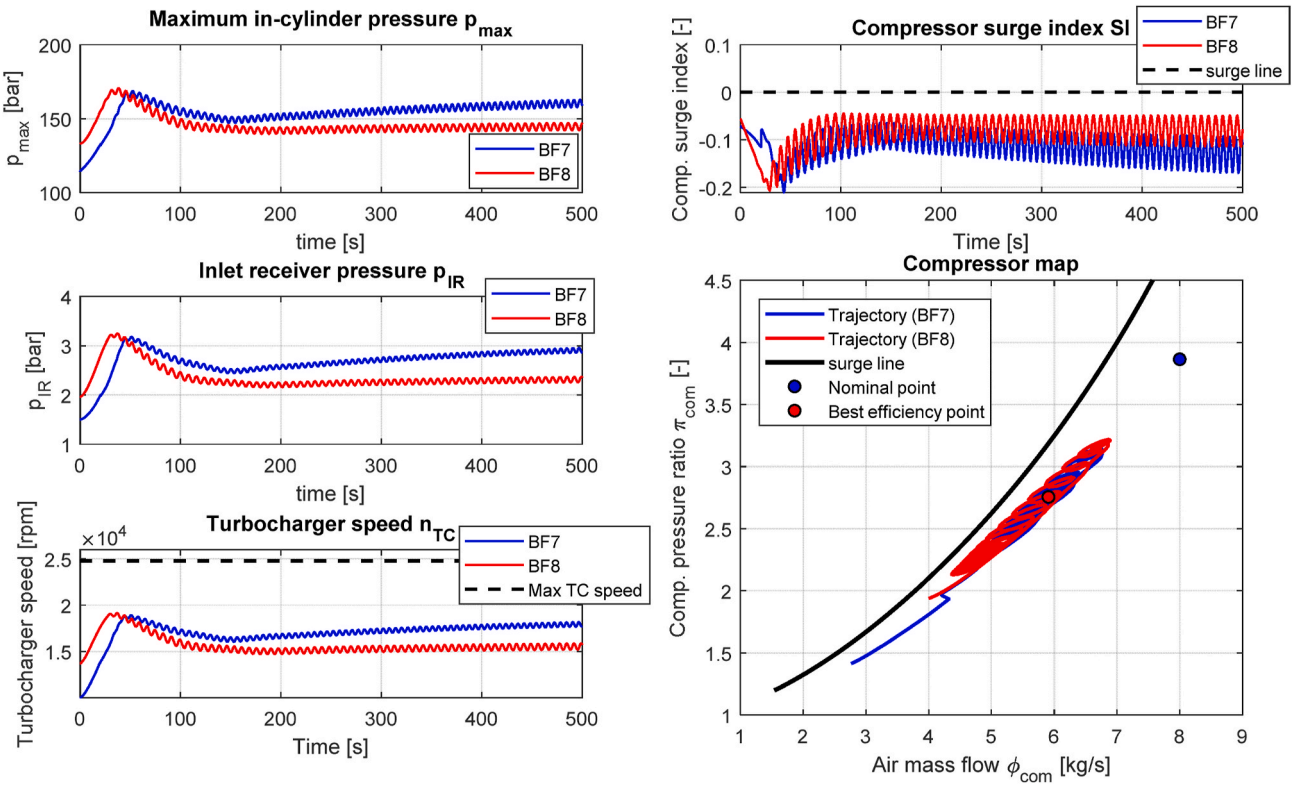

Fig. 23. Maximum in-cylinder pressure, inlet receiver pressure, turbocharger rotational speed, compressor surge index and compressor behaviour during ship turning to head sea.

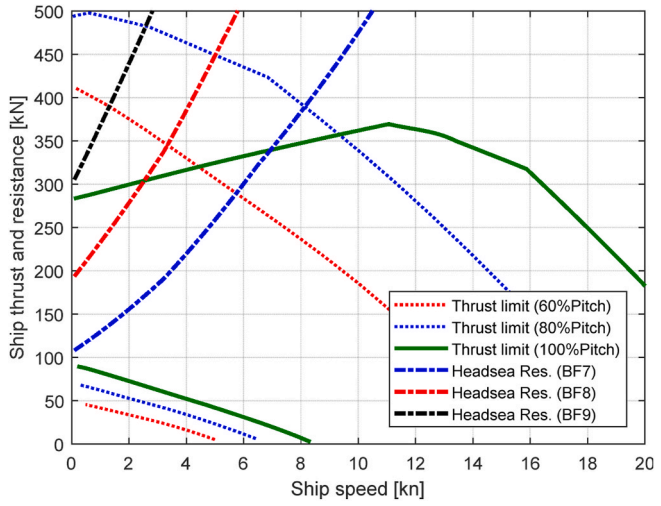

Fig. 24. Ship thrust envelope with different propeller pitches Limit lines at the bottom represent minimum engine rotational speed.

thus to reduce the engine thermal loading (Fig. 27).

6. Conclusions and recommendations

6.1. Conclusions

In this paper, based on the integrated ship propulsion, manoeuvring and sea state model, the ship propulsion and manoeuvring performance in adverse sea conditions (BF7 and BF8) has been investigated. The influence of the propeller pitch and the PTO/PTI on the ship thrust envelope have also been investigated. According to the simulation results, the maximum advance speed at which the benchmark chemical tanker is able to sail in head sea in sea state of BF7 is 7 knots, while in BF8 the maximum advance speed is 2.6 knots (but the engine will be highly thermally overloaded), and in BF9 the ship is not able to move forward at all. With an initial ship speed of 6.5 knots, the ship is able to turn to head wind and waves in both sea states of BF7 and BF8, while it cannot turn to head sea in BF9 since the ship speed drops to zero before that. According to the current 2013 interim minimum power guidelines, the specified adverse sea condition for the benchmark ship is sea state of BF7; and according to the level 2 assessment of the guidelines, the required ship advance speed is 6.4 knots. So, the benchmark ship meets the requirement of the level 2 assessment of the current guidelines, although it is an underpowered ship according to the level 1 assessment of the guidelines. Note that, as mentioned previously both the level 1 and level 2 assessments of the current guidelines are only applicable for ships with capacity over 20,000 DWT, although in this paper for the moment it is assumed that the guidelines are also applicable for the benchmark chemical tanker that has a capacity of 13,000 DWT. However, the contradictory results of the assessments of level 1 and level 2 for the benchmark chemical tanker shows the necessity of a proper minimum power guidelines for ships with capacity less than 20,000 DWT.

The wake fluctuation due to waves will cause fluctuations in propeller torque and thrust. Although the oscillating propeller thrust hardly has any influence on the ship motions due to the relatively big ship inertia, the fluctuating propeller torque does have notable impact on the engine behaviour. The fluctuating propeller wake will finally cause the fluctuations in engine speed, torque and thermal loading. Due to high sea state, for instance BF8, the engine could be thermally overloaded by the combined effects of the increasing steady loads and the fluctuating loads, even though the engine power or torque trajectories are still within the static operating envelope.

When transforming the engine power/revolutions envelope to ship thrust/velocity envelope, for the same engine envelope, using a different

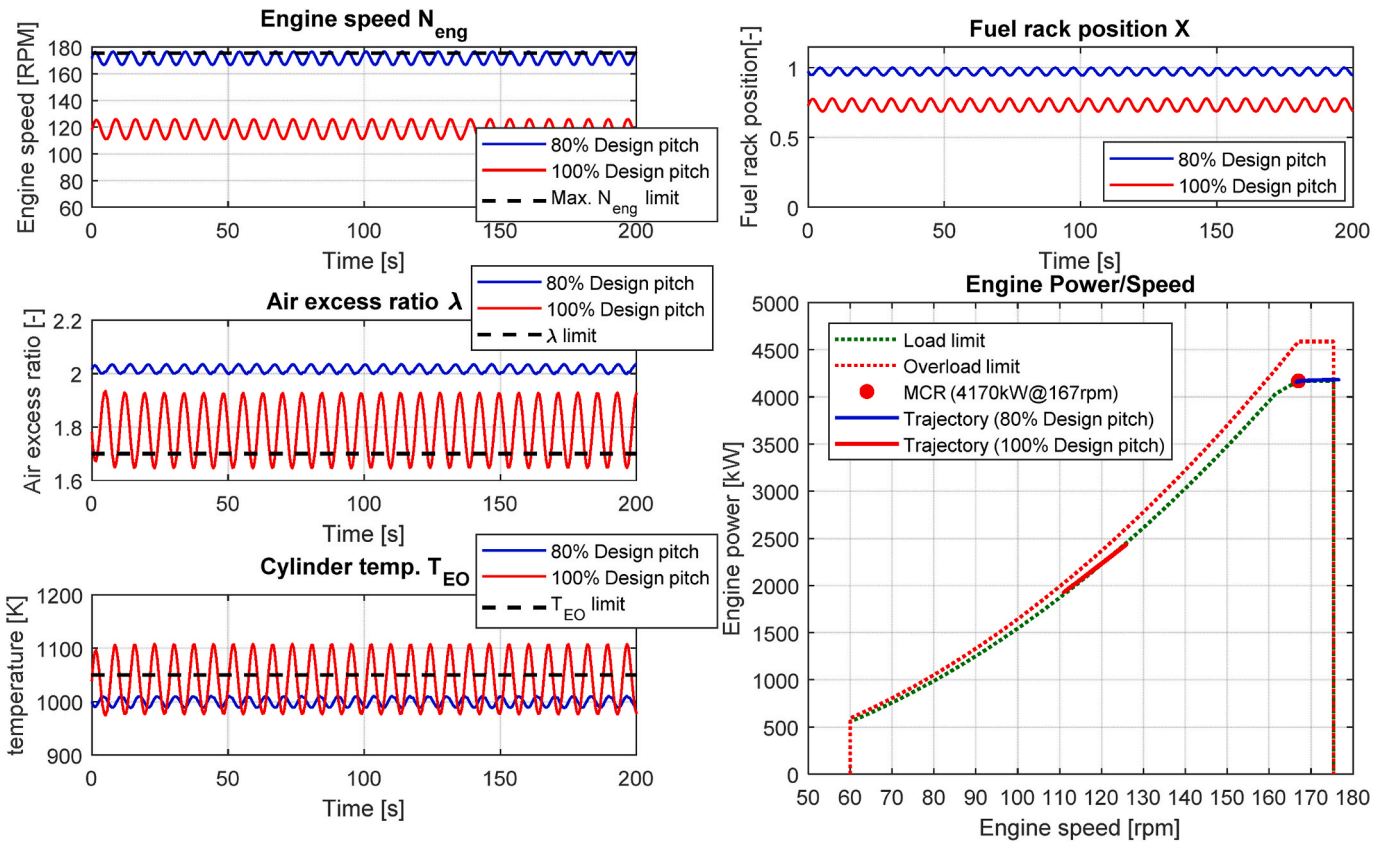

Fig. 25. Influence of reducing propeller pitch on engine performance when ship sailing in head sea in BF8.

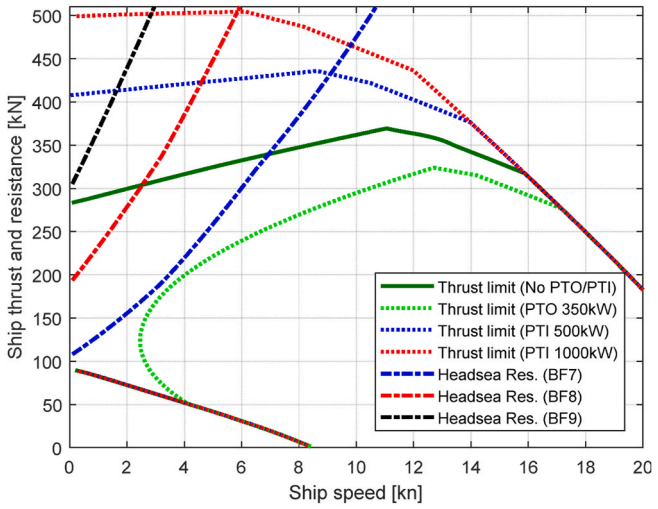

Fig. 26. Ship thrust envelope with PTO/PTI Limit lines at the bottom represent minimum engine rotational speed.

propeller or a different propeller pitch will lead to a different ship thrust envelope. For the same ship velocity, the engine could more easily exceed the thermal loading limit at high propeller pitches and overspeed at low pitches. That is why a good matching between the engine and propeller, and a good control of the engine and propeller especially under dynamic operations and/or in adverse weather conditions are very important from the operational safety point of view. A shaft generator (power-take-off, PTO) will narrow the ship thrust/velocity envelope but if the shaft generator can also work as a shaft motor (power-take-in, PTI) the ship thrust envelope can be widened. So, the shaft generator/motor can work as a generator in PTO mode when the ship sails in normal sea conditions for a better energy efficiency, while work as a motor in PTI mode when the ship needs more propulsion power especially in adverse weather conditions for a better operational safety of both the engine and ship.

6.2. *Recommendations*

Last but not least, there are still some limitations and uncertainties in this research. The following work is recommended for future research. To improve the accuracy of the predictions of the interactions between the ship propulsion plant, the ship and waves, etc., in high sea states, more accurate modeling of ship propulsion, manoeuvring and seakeeping is needed. For instance, the ship manoeuvring model used in this paper can be improved. To better capture ship behaviour in adverse sea conditions in a more realistic way, a 4 DOF (including ship rolling) or even 6DOF (including ship heaving and pitching) ship manoeuvring model could be used. The hydrodynamic coefficients in the manoeuvring and seakeeping models could be determined by experimental and advanced numerical methods. Although experimental and advanced numerical methods could be more accurate when estimating the wave-induced steady forces, a well-established and simple-to-use empirical method is very useful for practical applications. For instance, when detailed information of the hull form is not available, which is the case in this study, or in the early design stage, where the detailed hull form is still under development, an empirical method using a limited number of main ship particulars to satisfactorily capture the physical phenomena is preferred. Last but not least, further research should answer the question which aspect of thermal loading is most critical, the in-cylinder conditions (air excess ratio, max temperature and temperature before EO) or the after-cylinder conditions (exhaust valve, turbine inlet blades).

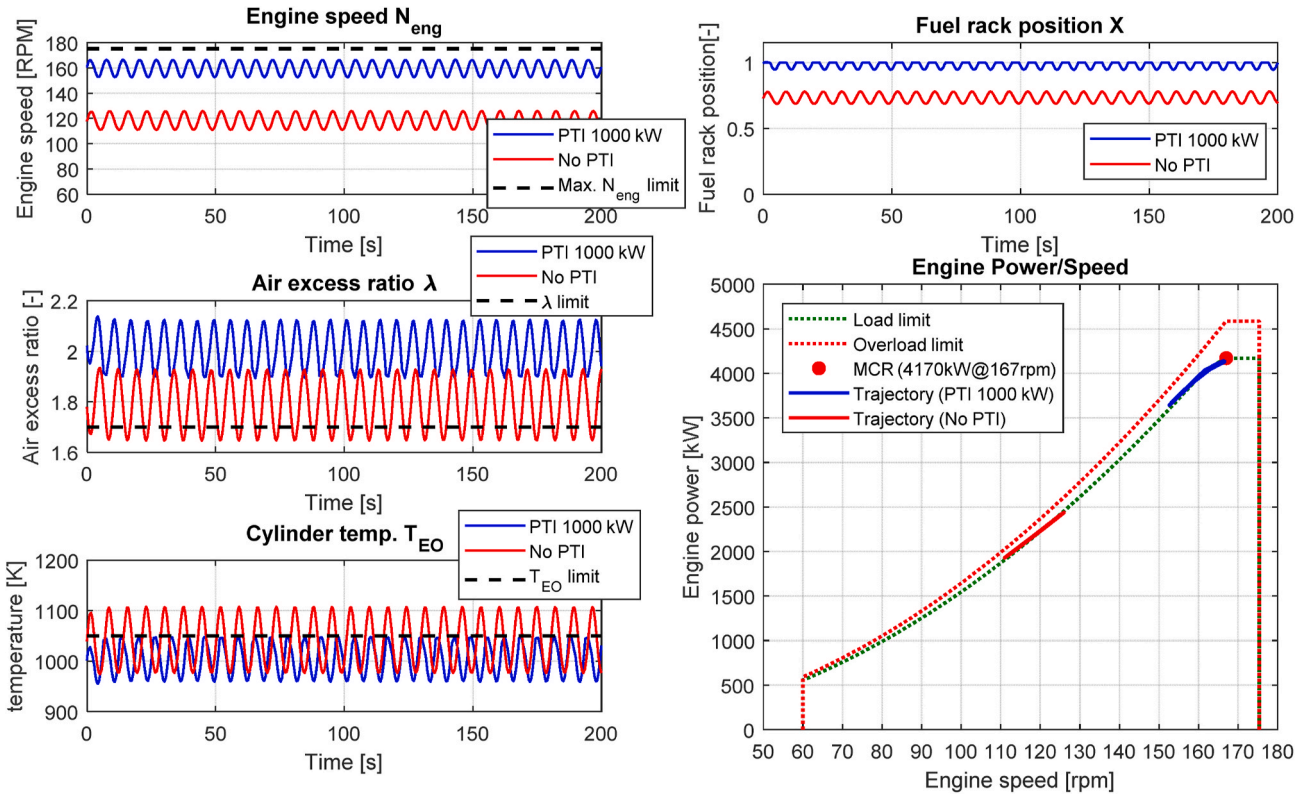

Fig. 27. Influence of PTI on engine performance when ship sailing in head sea in BF8.

CRediT authorship contribution statement

Congbiao Sui: Conceptualization, Software, Data curation, Visualization, Writing – original draft, Formal analysis, Investigation, Methodology. **Peter de Vos:** Formal analysis, Investigation, Methodology, Supervision, Validation, Writing – review & editing. **Hans Hopman:** Supervision, Writing – review & editing. **Klaas Visser:** Project administration, Writing – review & editing. **Douwe Stapersma:** Formal analysis, Investigation, Methodology, Validation, Writing – review & editing. **Yu Ding:** Resources, Funding acquisition, Writing – review & editing.

Declaration of competing interest

The authors declare that they have no known competing financial interests or personal relationships that could have appeared to influence the work reported in this paper.

Acknowledgements

This project partly is financially supported by the International Science and Technology Cooperation Program of China, 2014DFA71700; Marine Low-Speed Engine Project-Phase I; China High-tech Ship Research Program.

The authors would like to thank CSSC Marine Power Co., Ltd. (CMP) for providing the ample data of the benchmark ship and the engines, and the support for the measurements of the two-stroke marine diesel engines.

Appendix

The principal particulars of S-Cb84 (Table A. 1) and the averaged steady forces and moments coefficients of S-Cb84 in irregular waves calculated using SKFM (Figure A. 1). The averaged steady forces and moments coefficients of S-Cb84 in irregular waves shown in Figure A. 1 are calculated by using the strip theory-based Kochin-function method (SKFM) assuming a slender ship; the ITTC (International Towing Tank Conference) wave spectrum, and $\cos^2$ wave direction distribution function have been used (Yasukawa et al., 2019).

Table A
1: Principal particulars of S-Cb84 (Yasukawa et al., 2019)

Ship Length between perpendiculars L (m)	178.00
Breadth B (m)	32.26
Depth D (m)	14.46
Draught d (m)	11.57
Displacement volume ∇ (m^3)	55,810
Longitudinal position of the centre of gravity x_G (m) *	5.33
Block coefficient C_b (–)	0.84

* x_G is defined based on the midship and is positive when locating forward of midship. *.

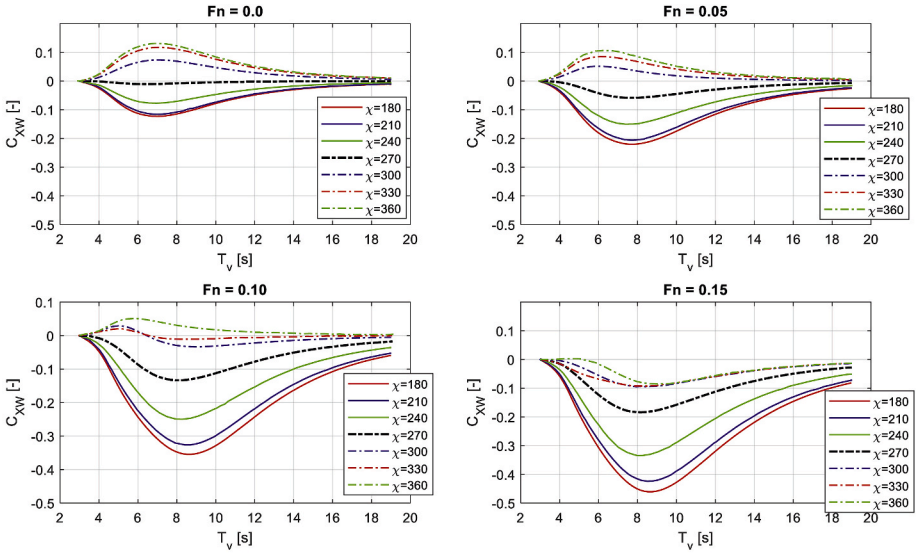

(a) Steady longitudinal force coefficients

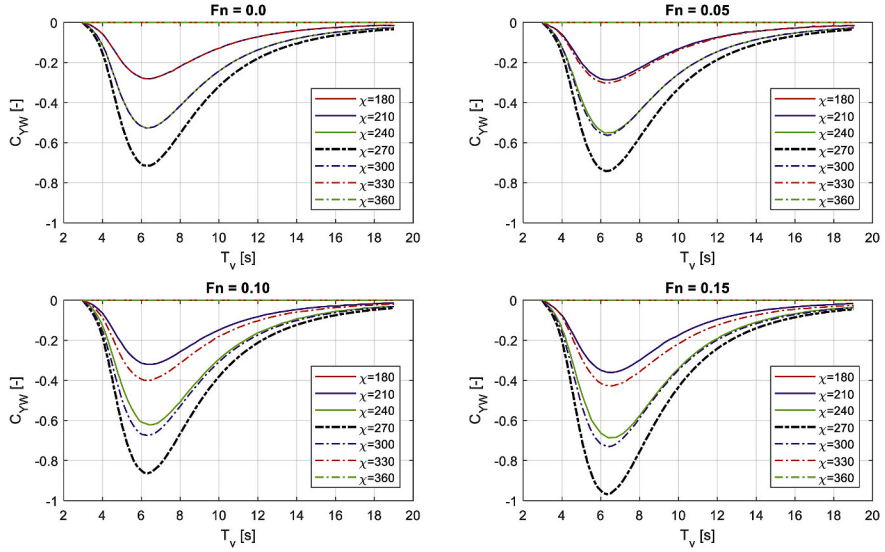

(b) Steady lateral force coefficients

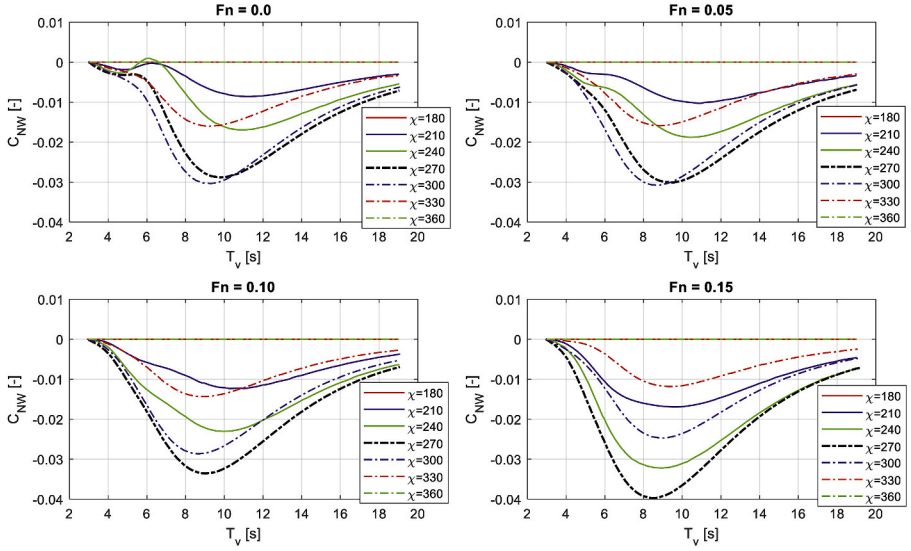

(c) Steady yaw moment coefficients

Fig. A.1. Averaged steady forces and moments coefficients of S-Cb84 in irregular waves calculated using SKFM (Yasukawa et al., 2019)

References

Abkowitz, M.A., 1964. Lectures on Ship Hydrodynamics: Steering and Manoeuvrability. Hydro- and Aerodynamic Laboratory. Lyngby, Denmark. No. Hy-5.

Aoki, I., et al., 2006. On the prediction method for maneuverability of a full scale ship (in Japanese). J. Jpn. Soc. Nav. Archit. Ocean Eng. 3, 157–165.

Aung, M.Z., Umeda, N., 2020. Manoeuvring simulations in adverse weather conditions with the effects of propeller and rudder emergence taken into account. Ocean Eng. 197, 106857.

Clarke, D., 1983. The application of manoeuvring criteria in hull design using linear theory. Trans RINA 125, 45–68.

Dallinga, R., et al., 2020. Low-powered ships in harsh weather. SWZ MARITIME 141 (2), 38–42.

Dirix, T., 2002. Renewed Concept Exploration Model for Manoeuvring. Master Thesis. Delft University of Technology, Delft, The Netherlands. https://repository.tudelft.nl/islandora/object/uuid:441d2d33-8d79-41b6-978d-56875d5a15c1.

Fossen, T.I., Wiley, I.O.S., 2011. Handbook of Marine Craft Hydrodynamics and Motion Control. Wiley, Chichester, West Sussex, U.K.

Fujiwara, T., et al., 2006. Cruising performance of a large passenger ship in heavy sea. San Francisco, California, USA. In: Proceedings of the Sixteenth International Offshore and Polar Engineering Conference. Paper Number: ISOPE-I-06-187.

Hasegawa, K., 1980. On a performance criterion of autopilot navigation. In: Journal of the Kansai Society of Naval Architects, 178. The Japan Society of Naval Architects and Ocean Engineers, pp. 93–103.

Holt, P., Nielsen, U.D., 2021. Preliminary assessment of increased main engine load as a consequence of added wave resistance in the light of minimum propulsion power. Appl. Ocean Res. 108, 102543.

IMO, 2016a. AIR POLLUTION and ENERGY EFFICIENCY - results of research project "energy efficient safe ship operation" (SHOPERA). MARINE ENVIRONMENT PROTECTION COMMITTEE, 70th session. MEPC 70/INF.33. https://edocs.imo.org/Final Documents/English/MEPC 70-INF.33 (E).docx.

IMO, 2016b. AIR POLLUTION and ENERGY EFFICIENCY - Report of JASNAOE Research Project for Determining Minimum Propulsion Power. MARINE ENVIRONMENT PROTECTION COMMITTEE, 70th session. MEPC 70/INF.35. https://edocs.imo.org/Final Documents/English/MEPC 70-INF.35 (E).docx.

IMO, 2019. ENERGY EFFICIENCY of SHIPS - Finalization of the Revised 2013 Interim Guidelines for Determining Minimum Propulsion Power to Maintain the Manoeuvrability of Ships in Adverse Conditions. MARINE ENVIRONMENT PROTECTION COMMITTEE, 75th session. MEPC 75/6/3.

Inoue, S., et al., 1981. A practical calculation method of ship maneuvering motion. Int. Shipbuild. Prog. 28 (325), 207–222.

ITTC, 2017. ITTC-recommended procedures and guidelines: full scale manoeuvring trials. In: Manoeuvring Committee of the 28th ITTC, 7.5-04-02-01.

Journee, J.M.J., et al., 2015. OFFSHORE HYDROMECHANICS, third ed. Delft University of Technology, Delft, The Netherlands.

Kijima, K., et al., 1990. On the manoeuvring performance of a ship with the parameter of loading condition. J. Soc. Nav. Archit. Jpn. 1990 (168), 141–148.

Kijima, K., et al., 2000. On a Prediction Method for Ship Manoeuvrability. In: The International Workshop on Ship Manoeuvrability-25 Years CPMC at HSVA. Hamburg.

Kijima, K., Nakiri, Y., 2002. On the Practical Prediction Method for Ship Manoeuvring Characteristics. Transactions of the West-Japan Society of Naval Architects, pp. 21–31.

Kijima, K., Nakiri, Y., 2003. On the Practical Prediction Method for Ship Manoeuvring Characteristics (In Japanese), 105. Transactions of the West-Japan Society of Naval Architects, pp. 21–31.

Kitamura, F., et al., 2017. Estimation of above water structural parameters and wind loads on ships. Ships Offshore Struct. 12 (8), 1100–1108.

Klein Woud, H., Stapersma, D., 2002. Design of Propulsion and Electric Power Generation Systems. IMarEST, Institute of Marine Engineering, Science and Technology, London.

Liu, J., 2017. Impacts of Rudder Configurations on Inland Vessel Manoeuvrability. PhD Thesis. Delft University of Technology, Delft, The Netherlands.

MEPC, 2011. Amendments to the Annex of the Protocol of 1997 to Amend the International Convention for the Prevention of Pollution from Ships, 1973, as Modified by the Protocol of 1978 Relating Thereto. MEPC 62/24/Add.1, Annex 19.

MEPC, 2013. 2013 interim guidelines for determing minimum propulsion power to maintain the manoeuvrability of ships in adverse conditions. MEPC 65/22. Annex 16.

MEPC, 2015. Amendments to the 2013 Interim Guidelines for Determining Minimum Propulsion Power to Maintain the Manoeuvrability of Ships in Adverse Conditions. MEPC 68/21/Add.1, Annex 7. https://edocs.imo.org/Final Documents/English/MEPC 68-21-ADD.1 (E).doc.

MEPC, 2017. 2013 interim guidelines for determining minimum propulsion power to maintain the manoeuvrability of ships in adverse conditions, as amended (resolution mepc.232(65), as amended by resolutions mepc.255(67) and mepc.262(68)). MEPC.1/Circ.850/Rev.2. https://doi.org/10.1093/ww/9780199540884.013.45058.

Mundt, T., et al., 2019. Overcoming the conflict of EEDI and minimum power for safe operation in adverse weather, the shaft power limitation - concept. In: CIMAC Congress 2019. Vancouver, Canada.

Ogawa, A., et al., 1977. MMG report-I, on the mathematical model of ship manoeuvring. Bull. Soc. Naval. Archit. Jpn 575 (22–28).

Papanikolaou, A., et al., 2016. Energy efficient safe SHip operation (SHOPERA). Transport. Res. Procedia 14, 820–829.

Psaraftis, H.N., 2019. Sustainable Shipping: A Cross-Disciplinary View. Springer, Cham, Switzerland.

Shigunov, V., 2018. Manoeuvrability in adverse conditions: rational criteria and standards. J. Mar. Sci. Technol. 23 (4), 958–976.

Shigunov, V., 2019. Assessment of maneuverability in waves. J. Ship Res. 63 (2), 78–93.

Shigunov, V., et al., 2019. Manoeuvrability in adverse conditions: case studies. Ocean Eng. 179, 371–386.

Shigunov, V., 2020. Practical assessment of manoeuvrability in adverse conditions. Ocean Eng. 203, 107113.

Smith, T.W.P., et al., 2015. Third IMO Greenhouse Gas Study 2014. International Maritime Organization (IMO), London, UK.

Sui, C., et al., 2019. Energy effectiveness of ocean-going cargo ship under various operating conditions. Ocean Eng. 190, 106473.

Sui, C., et al., 2020. Fuel consumption and emissions of ocean-going cargo ship with hybrid propulsion and different fuels over voyage. J. Mar. Sci. Eng. 8 (8).

Sui, C., et al., 2021. Mean value first principle engine model for predicting dynamic behaviour of two-stroke marine diesel engine in various ship propulsion operations. Int. J. Nav. Archit. Ocean Eng. 14, 100432.

Taskar, B., et al., 2016. The effect of waves on engine-propeller dynamics and propulsion performance of ships. Ocean Eng. 122, 262–277.

Ueno, M., et al., 2013. Estimation and prediction of effective inflow velocity to propeller in waves. J. Mar. Sci. Technol. 18 (3), 339–348.

UNCTAD, 2019. Review of Maritime Transport 2019. UNITED NATIONS PUBLICATION, Geneva.

Ventikos, N.P., et al., 2018. Statistical analysis and critical review of navigational accidents in adverse weather conditions. Ocean Eng. 163, 502–517.

WMO, 2019. Manual on Codes - International Codes - Volume I.1, Annex II to the WMO Technical Regulations, Part a - Alphanumeric Codes. World Meteorological Organization.

Yasukawa, H., et al., 2019. Evaluations of wave-induced steady forces and turning motion of a full hull ship in waves. J. Mar. Sci. Technol. 24 (1), 1–15.

Yasukawa, H., et al., 2021. Validation of 6-DOF motion simulations for ship turning in regular waves. J. Mar. Sci. Technol. 26, 1096–1111.

Yasukawa, H., Sakuno, R., 2020. Application of the MMG method for the prediction of steady sailing condition and course stability of a ship under external disturbances. J. Mar. Sci. Technol. 25 (1), 196–220.

Yasukawa, H., Yoshimura, Y., 2015. Introduction of MMG standard method for ship maneuvering predictions. J. Mar. Sci. Technol. 20 (1), 37–52.

Yoshimura, Y., Nomoto, K., 1978. Modeling of manoeuvring behaviour of ships with a propeller idling, boosting and reversing (in Japanese). J. Soc. Nav. Archit. Jpn. (144), 57–69, 1978.

Yum, K.K., et al., 2017. Simulation of a two-stroke diesel engine for propulsion in waves. Int. J. Nav. Archit. Ocean Eng. 9 (4), 351–372.

Zaky, M., et al., 2018. Improvement of maneuverability in a VLCC by a high lift rudder. Ocean Eng. 165, 438–449.

Zhang, C., et al., 2019. Experimental and numerical investigations of advancing speed effects on hydrodynamic derivatives in MMG model, Part I: xvv,Yv,Nv. Ocean Eng. 179, 67–75.